

Anonymous Referee #2

General Comments: The paper presents and analyzes surface level ozone over the U.S. Intermountain West for periods ranging from five to more than twenty five years, depending on the site. The writing is generally quite good, with few mistakes in grammar and usage. The authors have done a reasonable job of collecting, organizing, and analyzing data, but the presentation is quite heavy on details and not tightly focused enough for the average reader. That is to say, there is a small community that will benefit from the thorough work presented, but manuscript is full of site acronyms and numbers of all kinds, making it difficult to extract the conclusions the authors deem to be the most important. Unfortunately, I don't have an easy solution to fix this situation, but I encourage the authors to consider revising the paper in such a way as to de-emphasize the minute details and instead zero in on the most important take away points.

To enlarge upon this point, the impression this reader gets from the abstract is things are complicated and there are many factors that contribute to ozone concentrations and trends. Even within a moderately coherent region, trends vary from site to site. These variations are "likely", but not definitively linked to O&NG and other activities. I am not necessarily finding fault with the work and the findings, but the paper comes across as suggestive, rather than conclusive. As the authors reflect on the significant body of work they carried out, are there two or three (or four) key points they would like the scientific community and policy makers to learn from this work? I find the abstract too diffuse to pick out these points. The sentence on lines 40-43 is a case in point. First of all, it is a difficult sentence to read and understand due to the construction, and the "while" clause in particular. Second, is this nuanced finding important enough to be in the abstract? Are the authors suggesting emissions controls predicated on the phase of the AO? Is that in any way practical, either from a scientific or a regulatory perspective?

We would like to thank the reviewer for their constructive comments on our manuscript. We have taken most of the reviewer's suggestions to improve the manuscript. Below we have responded to each one of the reviewer's comments (shaded).

To make the manuscript more readable, we made the following revisions. First, acronyms that only appeared less than 4 times were deleted from the manuscript, such as Wyoming Department of Environmental Quality (WDEQ), Tropospheric Ozone Assessment Report (TOAR), and site acronyms (GRBA, ZION, GRCA, PEFO, BADL). Second, Table S1 in the supplement with sites' full names and acronyms were moved to the main text (Table 1). In addition, to further clarify locations of sites and O&NG extraction basins, we added 'MEVE was located to the northwest of San Juan Basin, while PNDE was located to the north of Green River Basin. Five sites are located *within* O&NG extraction basins. These five sites are: Canyonlands National Park (CANY) and Campbell, WY (CAMP), located within the Paradox Basin and Powder River Basin, respectively, Dinosaur National Monument (DINO), Rangely, CO (RANG), Meeker, CO (MEEK) within the Uintah Basin (Figure 1).' on Lines 160 – 166. Third, we have reorganized and edited substantially the manuscript to focus on the key findings of our study and to strengthen the support of those findings.

We revised the abstract to focus on three key points in this manuscript (Lines 25 – 50). First, emissions from O&NG extraction activities can alter decadal trends in Intermountain West O₃. Second, a 35% decrease of NO_x emissions from coal-fired electricity generation in eastern Utah caused decreasing O₃ design values there. Third, emission reductions in VOCs and NO_x in negative Arctic Oscillation (AO) winters and VOCs alone in positive ones can effectively mitigate O₃. ‘Box model simulations suggested that both volatile organic compounds (VOCs) and nitrogen oxides emission reductions during negative AO years while VOC emission reductions alone in positive AO years could effectively mitigate high wintertime O₃ within the O&NG basins.’ was changed to ‘Furthermore, emission reductions of volatile organic compounds (VOCs) and NO_x during negative AO years and VOC emission reductions alone in positive AO years could effectively mitigate high wintertime O₃ within the O&NG basins, as indicated by box model simulations.’ (Lines 43 – 46)

The goal of this paper is to identify factors that drive the long-term trends and variability in Intermountain West surface O₃ near O&NG extraction fields. Currently, there are either undocumented O&NG emissions or huge uncertainties in O&NG emissions (e.g., Thompson et al., 2017; Allen, 2014; Allen, 2016). In the future, multiyear studies with accurate emission inventories and three-dimensional chemical transport model simulations can further provide more practical numbers to reduce emissions of VOCs and NO_x to mitigate O₃.

Specific Comments: A problem with the paper that is easier to fix is the methodology for determining whether the trends they compute are “significant”. The authors perform a linear fit to the various data sets, then use the p values to impute the significance of the trends. The p value actually is a measure of how well the linear model fits the data. If the data were monotonically decreasing in a quadratic or exponential manner, the p value would be “poor” for the linear fit, but the trend would be undeniable. They need to use an appropriate statistical test for trends in the data if they want to evaluate the trend. The use of a Mann-Kendall test is a much more general way to do this. Of course, the authors use the slope from the linear model as their “trend estimate”, which is probably okay if Mann-Kendall shows that there is a significant trend, but this slope doesn’t have any real meaning if the trend itself is not significant. This should not be a difficult fix – and it may not change their results much, but it may. In any case it needs to be done properly!

Thanks for the suggestion. All trends were reported by the Mann-Kendall test now. Sen’s slope from Mann-Kendall analysis were used to estimate the trends (Lines 180 – 181). Tables S1-2 were updated. As the reviewer expected, the results did not change much and statistically significant trends were shown at the same sites from Mann-Kendall analysis and linear model.

Lines 173-175: To help put the study in perspective, the authors should report the decadal mean A4DM8HA for the Denver-Boulder and Salt Lake City metropolitan areas here.

Added “The decadal mean A4DM8HA O₃ was ~58 ppbv at the urban station CAMP in Colorado (<https://www.colorado.gov/airquality>) and ~77 ppbv at the urban station Hawthorne

in Utah (<https://deq.utah.gov/division-air-quality>)” to lines 215 – 217.

Lines 184-187: Is this sentence important to the paper? It is a very difficult sentence to digest, and it is not clear if there is any significance to the finding. If it is significant, take some time and explain it clearly. If not, omit it.

The sentence, “Overall seasonal median values near the O&NG extraction basins showed relatively more consistent patterns of interannual variation at relatively low elevation sites (i.e., CANY, DINO, MEEK, RANG, CAMP, MEVE, and WICA) in winter, while in summer, large differences were found between sites (Figure 3).” was changed to “Overall wintertime median values near the O&NG extraction basins showed relatively more consistent patterns of interannual variation with low O₃ values in 2012 and higher O₃ in 2011 and 2013 at relatively low elevation sites (i.e., CANY, DINO, MEEK, RANG, CAMP, MEVE, and WICA) (Figure 3).” (Lines 229 – 232). The detailed analysis can be found in Section 6.

Lines 236-37: Presumably this sentence refers to the CANY site only, although the text changes between site, basin and county get very confusing. The linear model computes a negative slope (decreasing trend), but the p value indicates the linear model does not fit the data well enough to fit the author’s criteria. I wonder if a Mann-Kendall test would indicate the presence of a trend? My gut feeling is yes.

The trend was reevaluated using Mann-Kendall analysis. Consistent with the linear model, no statistically significant trend was found in the 95th DM8HA O₃ at CANY from Mann-Kendall test (Table S2).

Line 423 and 889: Figure 10a-e is difficult to read. First of all, it would be helpful to the reader if in the title of panels a-e, there were an indication of whether the measurements took place in the summer or the winter. Example: “NACHTT(winter)”. Second, the authors should indicate on each panel (a-e again) the part of the day that was sunlit. Admittedly, over the course of each campaign the length of day varied. One way to indicate this would be to lightly shade the period between the earliest sunrise and the latest sunset, then use a slightly darker shading between the latest sunrise and the earliest sunset.

Thank you for the suggestions to help clarify the presentation in Figure 10. Seasons of field campaigns were added in Figure 10. Shaded areas were also added to indicate the time period between sunrise and sunlit. As the averaged diel cycle was simulated for each campaign, averaged daytime time period was marked in each figure.

Line 460-75 and 889: Figure 10f is presented with inadequate explanation. What do “NOx scaling factors” refer to? (How are they defined?) What is the base case VOC scenario? Where did it come from? Is it the same VOC mix and concentrations for all simulations? How does one interpret the sensitivity curve?

The following text was added:

‘Fifteen simulations for each field campaign were performed with observed VOC and NO_x mixing ratios, the latter (NO_x) of which were scaled by a factor varying from 0 to 5. NO_x scaling factor of 1 indicates observed NO_x mixing ratios (Figure 10f). The O₃ formation regime was found to be closely associated with the AO phase. Photochemically produced O₃ during UBWOS 2012 and UBWOS 2014 decreased with increasing NO_x mixing ratios, indicating VOC-limited O₃ formation regimes (Figure 10f).’ (Lines 576 – 583)

Lines 434-35: It seems unlikely to me that the mixing hypothesis is the only possible reason that the model and observations disagree! Either propose alternate possibilities, or qualify the favored hypothesis. (Or back it up.)

The box model used in this study served to simulate photochemically produced O₃, NOT ambient O₃ levels. In the model, we added turbulent mixing so that ambient concentrations of VOCs and NO_x were maintained (Lines 196 – 198 and Section S8). Therefore, simulated O₃ would be the product of photochemical reactions involving ambient VOCs and NO_x. The difference between simulated and ambient O₃ levels represented the combined impact of transport processes and stratospheric intrusion that were not represented in the chemistry box model as well as model uncertainties (Lines 539 – 540). When photochemically produced O₃ was higher than the observed value, the high O₃ amounts produced in situ would be reduced through dilution by mixing with surrounding clean air and ultimately lower values were observed. Therefore, the instantaneous mixing with surrounding air, which was not represented in the chemistry box model, was the reason that accounted for the difference between model outputs and observations.

Line 812: Figure 4 – panel b of this figure needs to be better explained to the reader. A simple sentence like the following added to the figure caption would be sufficient: “Yellow color indicates regions where NO_x has increased between 2005-2010 and 2011-2015, and blue color indicates regions where NO_x has decreased.”

Added.

Line 848: Figure 7 is too small to be useful. Perhaps a single example here, with better explanation, and move the rest to the supplement (also much bigger!). Explain in the figure caption or in the text the physical interpretation of the different color areas on the maps and cross sections.

We kept figures at ROMO and MEVE in the main text. The remaining figures were moved to Figure S4 in the supplement. ‘The red color indicates origins of air masses reaching the study site during high O₃ years, while the blue color indicates locations of major air mass sources during low O₃ years.’ was added to the caption.

Technical Corrections and/or Suggestions: Line 74: Suggest adding “winter” between “four” and “O₃”.

Added.

Line 76: Suggest adding “winter” between “6-day” and “high”.

Added.

Line 128: Add “of” between “upwind” and “O&NG”.

Added.

Line 137: Suggest deleting “the analysis of” – or similar rewording.

Deleted.

Line 189: Cooper et al., 2014 is not in the reference list.

Added.

Line 269: Please reword the passage “two U.S. largest”.

Changed to ‘Two largest natural gas fields in the U.S.’ (Lines 324 – 325)

Line 273: Add “and” before “reached”.

Added.

Lines 410-411: This sentence is confusing. “Stronger” than what?

Changed to ‘This indicates that cloudiness associated with precipitation weather had a stronger impact on summertime baseline O₃ than high percentile levels at sites within the basins.’ on Lines 368 – 370.

Line 454: NFR was used and defined back on line 78. I suggest eliminating the acronym and spelling out Northern Front Range all four times that it is used in the manuscript.

NFR was spelled out on Lines 110, 568, 569, 591.

Supplement:

Table S1: What is the meaning of the shadings? Please describe.

Table S1 was moved to the main text as Table 1. ‘Gray and blue shades indicate sites located outside of 100 km of shale plays. CRMO and YELL in blue shades are located upwind of O&NG extraction fields and used as reference sites.’ was added to Table 1.

Section S8.2: Equation E1 – I find it odd that $j(\text{NO}_2)$ does not go to zero in the absence of radiation. How can that be?

When the radiation went to zero, $j(\text{NO}_2)$ was $5.509 \times 10^{-6} \text{ s}^{-1}$, which was negligible. This value was derived from polynomial regression between downwelling solar radiation and $j(\text{NO}_2)$ data from the UBWOS2012 campaign. We remodeled their relationship with intercept set to 0, the coefficients did not change. The new equation was $j(\text{NO}_2) = 1.425 \times 10^5 \text{ Radiation}_{\text{downwelling}} + 4.760 \times 10^9 \text{ Radiation}_{\text{downwelling}}^2$

Table S8: Acronyms need to be spelled out.

Full names of acronyms used in Table S7 were listed after Table S7.

Reference:

Allen, D.T.: Atmospheric emissions and air quality impacts from natural gas production and use, *Annu. Rev. Chem. Biomol. Eng.* 5, 55-75, doi:10.1146/annurev-chembioeng-060713-035938, 2014.

Allen, D. T.: Emissions from oil and gas operations in the United States and their air quality implications, *Journal of the Air & Waste Management Association*, 66:6,549-575, DOI: 10.1080/10962247.2016.1171263, 2016.

Thompson, T. M., D. Shepherd, A. Stacy, M. G. Barna, and B. A. Schichtel: Modeling to Evaluate Contribution of Oil and Gas Emissions to Air Pollution, *Journal of the Air & Waste Management Association*, 67, 445-461, DOI:10.1080/10962247.2016.1251508, 2017.

1 **Decadal Trends and Variability in Intermountain West Surface Ozone near Oil and Gas**
2 **Extraction Fields**

3

4 Ying Zhou¹, Huiting Mao¹, and Barkley C. Sive²

5

6

7 ¹Department of Chemistry, State University of New York College of Environmental Science and
8 Forestry, Syracuse, NY, 13210, USA

9 ²National Park Service, Air Resources Division, Lakewood, CO 80225, USA

10

11 Corresponding author: H. Mao (hmao@esf.edu)

12

13

14

15

16

17

18

19

20

21

22

23

24 Abstract

25 Decadal trends in ~~the annual fourth highest daily maximum 8 hour average (A4DM8HA)~~ surface
26 ozone (O₃) were studied ~~over 2005 – 2015~~ for ~~13 rural/remote sites in~~ the U.S. Intermountain West.
27 ~~No over 2005 – 2015. Widely disparaging trends, or a lack thereof,~~ were ~~observed in A4DM8HA~~
28 ~~O₃ found~~ at ~~two reference~~ sites, ~~which are located upwind of and thus minimally influenced by~~
29 ~~emissions from~~ with sufficiently long data records, in/near oil and natural gas (O&NG) basins:
30 ~~Trends, or a lack thereof, varied widely at other 11 sites in/near O&NG basins~~ resulting from
31 different controlling factors rather than a simplistic, uniform one. ~~The~~ Three sites exhibited
32 statistically significant decreasing trends with rates of 0.83 ppbv/yr, -0.58 ppbv/yr, and -1.16
33 ppbv/yr at Mesa Verde ~~(-0.76 ppbv/yr)~~ and National Park, Canyonlands National Park ~~(-0.54~~
34 ~~ppbv/yr)~~, and Wind Cave National Park, respectively. It was found that the decreasing trends at
35 the first two sites were ~~attributed to a 37% decrease in~~ driven by decreased natural gas production
36 ~~in the San Juan Basin and 35% emission reductions in~~ and decreased emissions from coal-fired
37 electricity generation, ~~respectively. The decreasing nearby, and the~~ trend ~~(-1.21 ppbv/yr)~~ at Wind
38 Cave National Park resulted from reduced solar radiation due to increasingly frequent precipitation
39 weather. The lack of trends at the remaining sites was likely caused by the increasing O&NG
40 emissions and decreasing emissions from other anthropogenic activities. Wintertime
41 O₃ atmospheric stagnant ~~events~~ conditions, often with occurrence of high O₃, were associated with
42 the Arctic Oscillation (AO). ~~Box model simulations suggested that both~~ during the decade.
43 Furthermore, emission reductions of volatile organic compounds (VOCs) and ~~nitrogen oxides~~
44 ~~emission reductions~~ NO_x during negative AO years while and VOC emission reductions alone in
45 positive AO years could effectively mitigate high wintertime O₃ within the O&NG basins, as
46 indicated by box model simulations. Our findings suggest that emissions from O&NG extraction

47 ~~likely played a significant role in shaping long-term~~activities could alter decadal trends in
48 ~~surface~~Intermountain West O₃ ~~near/within O&NG basins~~design values and hence warrant
49 consideration in ~~the design of~~developing efficient O₃ mitigation strategies for the Intermountain
50 West.

51

52

53

54

55

56

57

58

59

60

61

62

63

64

65

66 1 Introduction

67 ~~—Tropospheric ozone (O_3) is a short lived trace gas that either originates naturally from the~~
68 ~~stratosphere (Stohl et al., 2003) or is produced in situ by photochemical oxidation of nitrogen~~
69 ~~oxides (NO_x) and volatile organic compounds (VOCs) or carbon monoxide (CO) (e.g., Monks et~~
70 ~~al., 2009). On 1 October 2015, the U.S. Environmental Protection Agency (EPA) lowered the~~
71 ~~National Ambient Air Quality Standard (NAAQS), namely the O_3 -design value, to 70 ppbv to~~
72 ~~improve protection of public health and welfare (EPA, 2015). Unlike in the eastern U.S., where~~
73 ~~NO_x -emission reductions have led to O_3 -declines, in the Intermountain West no decreasing trends~~
74 ~~were observed over 1988–2014 and surface O_3 could exceed the NAAQS in both winter and~~
75 ~~summer (Schnell et al., 2009; Cooper et al., 2012; Edwards et al., 2014; Lin et al., 2017). Most~~
76 ~~studies attributed the increasing background O_3 -trends over the western U.S. to increasing~~
77 ~~anthropogenic Asian emissions (e.g., Cooper et al., 2012; Parrish et al., 2012; Lin et al., 2017).~~
78 ~~Lefohn et al. (2012) found that stratospheric intrusion affected the interannual variability of surface~~
79 ~~O_3 at both high and low elevation sites. However, a multi-model study suggested that surface O_3~~
80 ~~in the U.S. was far more sensitive to domestic emission changes than to global emission changes~~
81 ~~in spring and summer (Reidmiller et al., 2009). Thus, long range transport from Asia and~~
82 ~~stratospheric intrusion may not be the sole contributors to the observed increasing trends in western~~
83 ~~U.S.—~~

84 ~~—Recent expanded use of horizontal drilling and hydraulic fracturing technologies enabled~~
85 ~~access to more natural gas resources in shale deposits (EIA, 2015). Tropospheric ozone (O_3) is~~
86 ~~a serious air pollutant that can be harmful to human and ecosystem health. Stratospheric intrusion~~
87 ~~and in situ photochemical oxidation of nitrogen oxides (NO_x), volatile organic compounds (VOCs),~~
88 ~~or carbon monoxide (CO) are two sources of tropospheric ozone (e.g., Stohl et al., 2003; Monks~~

89 et al., 2009). On 1 October 2015, the U.S. Environmental Protection Agency (EPA) lowered the
90 National Ambient Air Quality Standard (NAAQS), namely the O₃ design value, to 70 ppbv to
91 improve protection of public health and welfare (EPA, 2015). Unlike in the eastern U.S., where
92 NO_x emission reductions have led to declines in higher O₃ mixing ratios, in the Intermountain
93 West no decreasing trends were observed over 1988 – 2014, and surface O₃ exceeded the NAAQS
94 in both winter and summer (Schnell et al., 2009; Cooper et al., 2012; Edwards et al., 2014; Lin et
95 al., 2017).

96 Recent expanded use of horizontal drilling and hydraulic fracturing technologies enabled
97 access to more natural gas resources in shale deposits (EIA, 2015). Extraction of oil and natural
98 gas (O&NG) can result in the emission of O₃ precursor gases and subsequently episodes of
99 elevated O₃ mixing ratios in O&NG production basins frequently exceeding the NAAQS. (e.g.,
100 Schnell et al., 2009; Cheadle et al., 2017; Oltmans et al., 2019). Most notable were the episodes
101 that occurred during the cold season in the Intermountain West (Carter and Seinfeld, 2012;
102 Edwards et al., 2014; Rappenglück et al., 2014; Schnell et al., 2009). Carter and Seinfeld (2012)
103 ~~studied~~ found one of the four observed winter O₃ episodes studied to be highly NO_x-sensitive and
104 the other three VOCs-sensitive in the Upper Green River Basin in Wyoming ~~and found one episode~~
105 ~~highly NO_x-sensitive and the others VOCs-sensitive.~~ Edwards et al. (2014) ~~used~~, using a box
106 model to simulate a stagnant 6-day high winter O₃ event in the Uintah Basin ~~and found~~, suggested
107 that carbonyl photolysis was the dominant oxidant source. McDuffie et al. (2017) ~~studied O₃ in~~
108 ~~the Colorado Northern Front Range (NFR) in summer 2012 and found~~ estimated that O&NG
109 emissions contributed to 17% of the modeled maximum photochemically produced O₃. in the
110 Colorado Northern Front Range in summer 2012. To the best of our knowledge, ~~no~~ very few studies

111 have investigated the long-term impact of expanded O&NG extraction activities on surface O₃
112 over the intermountain U.S. using more than ten years of measurement data.

113 The effect of emissions from O&NG production on surface O₃ is difficult to quantify because
114 a wide range of factors work together to determine the mixing ratio of O₃ at a given location, such
115 as other anthropogenic emissions, natural emissions, transport processes, stratospheric intrusion,
116 O₃ photochemistry, and changing global climate (Parrish et al., 2013); ~~however~~. However, the
117 significance of these factors varies by season. For example, the number of high O₃ days in summer
118 was strongly correlated with wildfire burned area over the western U.S. as wildfires are important
119 sources of NO_x, CO, and VOCs (Jaffe et al., 2008; Jaffe and Wigder, 2012). The frequency and
120 intensity of wildfires in the western U.S. may behave been increasing, driven by increasing
121 temperatures, earlier snowmelt, drier conditions, and accumulation of fuels (Westerling et al., 2006;
122 Jaffe et al., 2008). Moreover, all components that can impact the distribution of O₃ are associated
123 with varying atmospheric circulation patterns on interannual to decadal ~~time~~-scales (e.g., Lin et al.,
124 2014; Zhou et al., 2017). For instance, model simulations suggested that more frequent
125 stratospheric intrusion events occurred in late spring, when the polar jet meandered towards the
126 western U.S. following La Nina events (Lin et al., 2014). Therefore, it is fundamentally important,
127 yet ~~also~~-challenging, to ~~extract~~delineate the impact of increasing emissions from O&NG
128 production on surface O₃ ~~levels~~ ~~from~~ ~~all~~ ~~of~~ ~~these~~ various factors. ~~However, these, and the~~
129 resultant findings could ultimately ~~lead~~contribute to improved modeling and to better assess the
130 efficacy of emission controls.

131 A most common approach to assess the influence of a certain factor or source on O₃
132 concentrations is through model simulations (e.g., Rodriguez et al., 2009; Lin et al., 2017).
133 However, the application of current chemical transport models used to investigate the impact of

134 emissions from O&NG extraction on tropospheric O₃ is particularly challenging because of ~~the~~
135 ~~large incomplete inventories of O&NG emission sources and huge~~ uncertainties ~~in~~ existing ~~in the~~
136 emission inventories ~~of O&NG extraction~~ (Páron et al., 2014; Helmig et al., 2014; Ahmadov et
137 al., 2014; Thompson et al., 2017; Allen, 2014; Allen, 2016). ~~Past studies have found that~~ A case in
138 point is the largely underestimated emissions of methane and VOCs from ~~oil and gas~~ O&NG
139 extraction ~~was largely underestimated (as suggested by~~ Karion et al., (2013); ~~and~~ Ahmadov et
140 al., (2014). ~~—~~ Consequently model simulations can be difficult to interpret. Therefore, for this
141 study the approach of *data analysis* was chosen ~~in order~~ to provide measurement-based
142 ~~contribution estimates~~ understanding of how O&NG emissions together with various factors may
143 have worked together to shape the long-term variation in Intermountain West surface O₃.

144 Specifically, we investigated the decadal impact of emissions from O&NG extraction on
145 variability and long term trends ~~of surface O₃ in the~~ Intermountain West surface O₃ since 2005,
146 when O&NG extraction activities started to expand rapidly (EIA, 2015). In this study, we used
147 long term O₃ measurement data obtained from the National Park Service ~~(NPS)~~,₂ Clean Air Status
148 and Trends Network ~~(CASTNET)~~,₂ and Wyoming Department of Environmental Quality
149 ~~(WDEQ)~~,₂ many of which are from Class I areas as designated by the Clear Air Act. ~~However,~~
150 ~~some~~ Some of these sites have been reportedly influenced by O&NG emissions since 2005 (EIA,
151 2015). This study was focused on the summer and winter, when NAAQS exceedances ~~of NAAQS~~
152 tended to occur in the Intermountain West (Edwards et al., 2014; Lin et al., 2017).

153 **2 Materials and Methods**

154 **2.1 Site Selection and Data description**

155 Long term surface O₃ observations were available at 18 sites in remote and rural areas of the
156 U.S. Intermountain West (Figure 1 and Table S11). Among the 18 sites, 11 sites are located within

157 100 km of a shale play and are more likely affected by emissions from O&NG extraction activities
158 (Figure 1). Specifically, Six sites, Mesa Verde National Park (MEVE), Pinedale, WY (PNDE),
159 Centennial, WY (CNTL), Gothic, CO (GTHC), Rocky Mountain National Park (ROMO), and
160 Wind Cave National Park (WICA), are located ~~near O&NG Basins~~ outside O&NG basins. MEVE
161 was located to the northwest of San Juan Basin, while PNDE was located to the north of Green
162 River Basin. Five sites are located within O&NG extraction basins. These five sites are:
163 Canyonlands National Park (CANY), and Campbell, WY (CAMP), located within the Paradox
164 Basin and Powder River Basin, respectively, Dinosaur National Monument (DINO), Rangely, CO
165 (RANG), Meeker, CO (MEEK), ~~and Campbell, WY (CAMP) are located~~ within ~~O&NG~~
166 ~~basins~~, the Uintah Basin (Figure 1). Of the remaining 7 sites, Yellowstone National Park (YELL)
167 and Craters of the Moon National Monument and Preserve (CRMO) were the only two sites
168 located upwind of O&NG fields and were therefore used as reference sites to investigate the
169 decadal O₃ change with minimal influence of O&NG emissions. Four sites, Great Basin National
170 Park (~~GRBA~~), Zion National Park (~~ZION~~), Grand Canyon National Park (~~GRCA~~), and Petrified
171 Forest National Park (~~PEFO~~), were found, based on backward trajectory cluster analysis, to often
172 receive air masses influenced by nearby anthropogenic emissions from Las Vegas (Section S2).
173 Badlands National Park (~~BADL~~), located more than 100 km away from the shale play, was
174 impacted one third of the time by air masses from O&NG activity in the Powder River Basin
175 during the 2005 – 2015 decade (Section S2). Therefore, ~~GRBA, ZION, GRCA, PEFO and~~
176 ~~BADL~~ the above five sites were not included in ~~the analysis of~~ this study.

177 Continuous hourly measurements of O₃ were available at each site. We calculated the
178 annual fourth-highest daily maximum 8-hour average (A4DM8HA), upon which the O₃ design
179 value was based, for the 13 monitoring sites ~~and their trends were examined through ordinary~~

180 ~~linear least-square regression.~~ Trends (ppbv yr⁻¹) in A4DM8HA were then reported using Sen's
181 ~~slopes from non-parametric Mann-Kendall analysis.~~ The trends were also calculated separately for
182 5th, 50th, 95th percentiles of daily maximum 8-hour average (DM8HA) O₃ in winter and summer.

183 2.2 Box Model Simulations

184 Box model simulations were performed using BOXMOX (Knote et al., 2015) and the NCAR
185 Tropospheric Ultraviolet and Visible Radiation Model (TUVv5.3.1) (Madronich et al., 1998).
186 BOXMOX is an extension to the Kinetic PreProcessor which allows ~~an~~-easy set-up for ~~zero~~
187 ~~dimension~~ box model simulations (Knote et al., 2015). We selected the Master Chemical
188 Mechanism (MCM v3.3) for the model chemistry scheme. The MCM is a near-explicit chemical
189 mechanism including gas-phase tropospheric degradations of 74 VOCs and OVOCs with a total
190 of 5259 species of and 15176 reactions (Jenkin et al., 2015).

191 All simulations were initialized with observations from field campaigns in the Intermountain
192 West- ~~during the study period.~~ These campaigns were Uintah Basin Winter Ozone Study (UBWOS)
193 over 2012 – 2014 (Edwards et al., 2013), Nitrogen, Aerosol Composition, and Halogens on a Tall
194 Tower (NACHTT) in 2011 (Swarthout et al., 2013), and Front Range Air Pollution and
195 Photochemistry Experiment (FRAPPÉ) in 2014 (Pfister et al., 2017). Section S8 provides detailed
196 information ~~about~~on field campaign measurements. The modeled mixing ratios of CO, CH₄, NO,
197 NO₂, and non-methane VOCs were forced to match the measured diurnal profiles by introducing
198 turbulent mixing to the model (Knote et al., 2015; Section S8.3). Therefore, the “box” can
199 dynamically exchange with its surroundings. The model was integrated forward with a time step
200 of 10 minutes until the concentrations reach a diurnal steady state, when the cycles of simulated
201 species exhibit less than 0.01% variation from the previous day (Edwards et al., 2013). The last 24

202 h were used to represent the simulated diel cycles. Section S8 provides further information on the
203 model treatment of all chemical observations.

204 3. General Characteristics in Long-term Variations of O₃

205 First, changes in the A4DM8HA ~~were examined for the 13 sites from~~ before ~~and to~~ after 2005,
206 when O&NG extraction started expanding rapidly, ~~were examined for the 13 sites. Note that trends~~
207 ~~were not calculated for three sites, DINO, RANG, and MEEK, due to short data records (<6 yrs)~~
208 ~~or too many missing data~~. Before 2005, statistically significant increasing trends were observed at
209 the reference site CRMO as well as ~~three other sites~~, CANY, CNTL, and PNDE, ~~three sites~~ near
210 O&NG basins ~~with, and~~ no significant trends ~~were observed~~ at the ~~other remaining five~~ sites
211 (Figure 2; ~~Table S1~~). After 2005, no significant trends were found at the two reference sites
212 (CRMO and YELL, ~~Table S2~~), ~~and decreasing or no trends were found at the Height~~
213 sites near/within the O&NG basins. ~~Specifically~~, significant decreasing trends were observed at
214 CANY (-0.5458 ppbv yr⁻¹), MEVE (-0.7683 ppbv yr⁻¹), and WICA (-1.2416 ppbv yr⁻¹), ~~with while~~
215 no significant trends at the other ~~five sites~~ (Table ~~S2~~S1). The ~~decadal mean A4DM8HA O₃ was~~
216 ~~~58 ppbv at the urban station CAMP in Colorado (<https://www.colorado.gov/airquality>) and ~77~~
217 ~~ppbv at the urban station Hawthorne in Utah (<https://deq.utah.gov/division-air-quality>). In comparison,~~
218 ~~the~~ decadal (2005 – 2015) mean of the A4DM8HA reached or exceeded 70 ppbv, the current
219 NAAQS, at three sites, DINO (82.7 ppbv), RANG (72.7 ppbv), and ROMO (75.1 ppbv).

220 Trends in seasonal 5th, 50th, 95th percentiles of DM8HA O₃ were further examined ~~for winter~~
221 ~~and summer seasons~~ (Table ~~S3~~S2). At the two reference sites, no trend was observed in any
222 seasonal percentiles of DM8HA O₃ at YELL, while statistically significant decreasing trends (-
223 0.1416 to -1.1830 ppbv yr⁻¹) were observed in wintertime 50th/95th and summertime 5th/50th/95th
224 percentile values at CRMO. Significant decreasing trends were also observed at 4 sites located

225 in/near O&NG basins. Specifically, at MEVE significant decreasing trends of ~~-0.4947~~ to ~~-0.6369~~
226 ppbv yr⁻¹ were found in seasonal 50th/95th percentile values in both winter and summer (Table S3).
227 In contrast, significant decreasing trends were only found in summertime 5th/50th at CANY,
228 summertime 95th at WICA, and wintertime 50th/95th percentile values at GTHC. Overall
229 ~~seasonal~~wintertime median values near the O&NG extraction basins showed relatively more
230 consistent patterns of interannual variation with low O₃ values in 2012 and higher O₃ in 2011 and
231 2013 at relatively low elevation sites (i.e., CANY, DINO, MEEK, RANG, CAMP, MEVE, and
232 WICA) ~~in winter, while in~~(Figure 3). In summer, large differences were found between sites
233 (Figure 3).

234 Previous studies have examined long term trends in tropospheric O₃ for varying time
235 periods over the continental U.S. (e.g., Cooper et al., 2012; Cooper et al., 2014; Lin et al., 2017;
236 Gaudel et al., 2018). Gaudel et al. (2018) assessed surface O₃ trends at 2702 non-urban sites ~~from~~
237 ~~the Tropospheric Ozone Assessment Report (TOAR) database. They found significant~~
238 ~~increasing and did not find~~ trends ~~(0.5 to 1.0 ppbv yr⁻¹) in daytime average O₃ at 6 sites in the~~
239 ~~Intermountain West and no trends at 8 other~~at sites including MEVE, PNDE, YELL in winters of
240 2000 – 2014 ~~(Gaudel et al. 2018)~~. However, in this our study a significant decreasing trend (-
241 ~~0.4967~~ ppbv yr⁻¹) in wintertime 95th percentile values was observed at MEVE after 2005, possible
242 causes for which ~~are discussed further~~were examined in Section 4. In summers of 2000 – 2014,
243 significant decreasing trends (~ -0.5 ppbv yr⁻¹) in daytime average O₃ were observed by Gaudel et
244 al. (2018) at most sites including CRMO, PNDE, CANY, MEVE, which was consistent with the
245 trends ~~we observed~~ for our study period 2005 – 2015 (Table S3).

246 The following questions arose from examining the above characteristics in surface O₃ at
247 the 11 sites near/in O&NG basins:

248 1) ~~Were~~How were the decreasing trends in A4DM8HA at MEVE, CANY, and WICA
249 ~~potentially and no trends at other sites~~ linked ~~in some ways to~~ changes in nearby O&NG
250 production activities ~~nearby~~?

251 2) Was ~~there seasonal variation in~~ the influence of emissions from O&NG extraction on
252 ~~seasonal~~ DM8HA O₃ seasonally variable?

253 3) Were there changes of O₃ production regime as a result of emissions from O&NG basins
254 over the years?

255 These questions ~~are~~were addressed in the following sections with the goal to delineate the role of
256 emissions from O&NG production in long-term trends in surface O₃ at the 11 sites.

257 **4. Contribution of emissions from O&NG production vs other anthropogenic sources**

258 The two reference sites, YELL and CRMO, are located >100 km upwind of O&NG basins
259 (Figure 1) and exhibited no trends in A4DM8HA after 2005. In comparison, ~~decadal trends of~~
260 O₃ varied widely at the ~~Height~~ sites situated in or near ~~the~~ O&NG extraction basins ~~ranged widely,~~
261 ~~indicating~~. The following analysis suggests that such varying trends resulted from the complex
262 influence of varying ranges of changes in emissions from O&NG production activities combined
263 with other anthropogenic sources.

264 The four low-elevation sites, MEVE, CANY, WICA, and CAMP, were situated near/within
265 O&NG basins, with the first three showing significant decreasing trends and the last none. The
266 strong decreasing trends in A4DM8HA at MEVE and CANY appeared to be driven by significant
267 reductions of emissions from local industry during 2005 – 2015. MEVE is located near the San
268 Juan Basin (Figure 1), the second largest natural gas field in the U.S. ~~A., where a~~ 37% decrease
269 ~~in~~was reported for its natural gas production ~~was reported in the San Juan Basin~~ over 2005 – 2015
270 (Figure 4a),) subsequently leading to reduced emissions of O₃ precursors. Meanwhile NO_x

271 emissions from other sectors in San Juan County decreased by 65% from 80,734 tons in 2005 to
272 27,996 tons in 2014 (Table S4). This is supported by the strong declines in tropospheric NO₂
273 column densities in summer at a rate of $\sim -2.8 \times 10^{13}$ molecular cm⁻² yr⁻¹ ($p \leq 0.05$) surrounding
274 MEVE around the San Juan Basin over 2005 – 2015 (Figure 4b). Decadal changes were not
275 computed for winter due to scarce wintertime column NO₂ retrievals over the Intermountain West.
276 Because O₃ production in U.S. rural areas was typically sensitive to changes in NO_x emissions
277 (Cooper et al., 2012), the decreasing NO_x emissions associated with reduced natural gas production
278 and emission controls in other sectors were most likely the primary cause for the significant
279 decrease in the A4DM8HA at MEVE (-0.7683 ppbv yr⁻¹) during 2005 – 2015. The significant
280 decreasing trend in the A4DM8HA observed at CANY was possibly a result of the declining
281 extraction of coalbed methane (CBM) in the Paradox Basin and emission reductions in coal-fired
282 electricity generation in Emery County. Historically, Emery County in the Paradox Basin was the
283 main CBM producer. ~~Permitting activities for~~ CBM extraction ~~have~~has declined by 48% over 2005
284 – 2015 resulting from lower natural gas prices (NGI, 2018) (Figure 4a). Meanwhile, NO_x emissions
285 from coal-fired electricity generation, contributing ~88% of the total NO_x emissions in Emery
286 County, decreased by 35% from 28,407 tons in 2005 to 18,336 tons in 2014 (Table S4). ~~As a result~~
287 ~~of these changes, significant decreasing trends in the seasonal 95th percentile would be anticipated,~~
288 ~~but were not observed in both winter and summer. This indicates that there are additional factors~~
289 ~~producing significant influences on O₃ in the area, which are further investigated in Sections 5–~~
290 ~~6.S3).~~

291 ~~No trend was observed in the A4DM8HA O₃ at CAMP, which was~~WICA, located
292 downwind of the Powder River Basin, also experienced a significant decreasing trend in the
293 A4DM8HA at a rate of 1.16 ppbv yr⁻¹ ($p = 0.09$) over 2005 – 2014. Curiously, total NO_x emission

294 increased by 29% from 1,327 tons in 2005 to 1,712 tons in 2014 in Custer County, where WICA
295 is located (Table S3). The decreasing A4DM8HA at WICA indicates additional factor(s) with
296 significant influences, which were further investigated in Sections 5. CAMP, located within the
297 Powder River Basin, saw no trend in the A4DM8HA O₃, likely associated with changes in natural
298 gas vs. oil production activities in the Powder River Basin. ~~CAMP is located within the~~The Powder
299 River Basin, ~~which~~ is traditionally known for its coal production and has been one of the fastest
300 growing oil producing regions in recent years. While natural gas production in Campbell County
301 decreased by 62% (Figure 4a), oil production in Campbell County increased from 9×10⁸ barrels in
302 2005 to 2.3×10⁹ barrels in 2015 (<http://wogcc.wyo.gov/>). ~~WICA is located downwind of the~~
303 ~~Powder River Basin, experiencing a significant decreasing trend in the A4DM8HA at a rate of~~
304 ~~1.21 ppbv yr⁻¹ (p = 0.05) over 2005–2014. Curiously, total NO_x emission increased by 29% from~~
305 ~~1,327 tons in 2005 to 1,712 tons in 2014 in Custer County, where WICA is located (Table S4).~~
306 ~~The decreasing A4DM8HA at WICA is attributed to other factors, as discussed in Section 6.~~

307 ~~DINO, RANG, and MEEK are located within the Uintah-Piceance Basin O&NG fields~~
308 ~~(Figure 1). Increased emissions, most likely from a 68% rise in natural gas production over 2005~~
309 ~~–2015 in the Uintah Basin (Figure 4a), together with snow cover (Edwards et al. 2014; Section~~
310 ~~xx), could have contributed to very high A4DM8HA O₃ at DINO and RANG. Meanwhile, NO_x~~
311 ~~emissions from highway vehicles decreased by 86% in Uintah County (Table S4). MEEK, in Rio~~
312 ~~Blanco County, is located at the eastern edge of the Piceance Basin and relative lower 4DM8HA~~
313 ~~O₃ (64.1 ppbv) was observed, and trends were not examined for the site's short data record (6 yrs).~~

314 The four *high*-elevation sites, ROMO, PNDE, CNTL, and GTHC, experienced no trends
315 in their A4DM8HA due likely to opposite changes in emissions from O&NG production, urban
316 sources, and stratospheric intrusion (or a lack thereof). ROMO is located to the west of the

317 Denver-Julesburg Basin and has experienced northwesterly and southeasterly wind most
318 frequently over 2005 – 2015 (Figure 5a) with higher O₃ (>60 ppbv) from the east and southeast
319 (Figure 5e). Natural gas production in Weld County increased by nearly a factor of 3 from 2009
320 to 2015, which coincided with use of horizontal drilling starting in 2009 (Figure 4a). Meanwhile
321 ~~the~~ NO_x emission ~~reductions~~reduction of ~37% from the urban area of Denver offset the effect
322 of increased NO_x emissions from O&NG extraction, as evidenced by the significant declines in
323 tropospheric column NO₂ (Figure 4b).

324 PNDE is located to the north of the Green River Basin, which has two ~~U.S.~~ largest natural gas
325 fields; in the U.S., i.e., Pinedale Anticline and Jonah Field. Natural gas production increased
326 steadily over 2005 – 2010 followed by a decline in 2011 and onward. ~~At PNDE, while the~~The
327 dominant winds at PNDE were from the northwest, ~~southeast~~southwest, and northeast (Figure 5b);~~).~~
328 However, O₃ mixing ratios ~~corresponding to~~in the southwesterly wind, ~~from~~ where expansive
329 O&NG extraction occurred, ~~reached higher than~~can exceed 60 ppbv (Figure 5f). Overall, no trend
330 was observed in natural gas production in Sublette County in the basin (Figure 4a), which was
331 consistent with the relative constant A4DM8HA at PNDE.

332 CNTL was located to the north of the North Park Basin and southeast of the Green River Basin
333 (Figures 1 and 5g). In the past decade, natural gas production in Jackson County in the North Park
334 Basin decreased by 72% (Figure 4a) and oil production increased comparatively by 73%, which
335 likely contributed to constant A4DM8HA O₃ at CNTL. ~~Similar to all high elevation sites (i.e.,~~
336 ~~ROMO, PNDE, CNTL),~~ GTHC ~~is another site,~~ located at on the mountain ridge. ~~The,~~ saw high O₃
337 concentrations from the north (> 65 ppbv) and southwest (> 52 ppbv) ~~indicate that the site was~~
338 ~~likely under the influence~~indicating combined influences of aforementioned opposite changes in

339 emissions from the North Park Basin, Denver-Julesburg Basin, and San Juan Basin (Figures 5d
340 and h) ultimately resulting in ~~the site exhibiting~~ no trend in the A4DM8HA.

341 **55. Effects of precipitation weather on summertime O₃**

342 We found that summertime O₃ in the Intermountain West was strongly correlated with
343 relative humidity and the wildfire index total fire index (Table S5). Studies have suggested that in
344 the Intermountain West, summertime O₃, especially the seasonal high percentile levels, was
345 impacted by photochemical production from wildfire emissions (Table S5; Jaffe and Wigder, 2012;
346 Lu et al., 2016). To avoid repeating the extensive body of literature on this topic, our own analysis
347 of the effect of wildfires on O₃ can be found in Section S5. One key point coming out of our
348 analysis was, with fire influence removed as indicated in partial correlation, significant negative
349 correlations between summertime O₃ and relative humidity were found at the two reference sites
350 (CRMO and YELL), as well as at the seven O&NG emission influenced sites (CANY CAMP,
351 MEEK, RANG, ROMO, PNDE, and WICA) (Table S5). Further investigation, detailed as follows,
352 revealed that this correlation essentially illuminated the effect of reduced solar radiation on O₃
353 production caused by cloudiness associated with precipitation weather.

354 In the Intermountain West, precipitation varies by elevation and latitude among other
355 factors (Williams et al., 1962). The decadal summertime average precipitation abundance was
356 larger at YELL (reference site, 0.17 kg m⁻²), GTHC, CNTL, ROMO, and WICA (0.15 – 0.27 kg
357 m⁻²) than that at CRMO (reference site, 0.08 kg m⁻²) and the remaining sites (Figure 6a). Further
358 examination revealed that YELL, GTHC, CNTL, ROMO, and WICA are located at much higher
359 elevation up in the mountains, where localized convective storms could develop quickly in summer
360 leading to higher precipitation amounts (Williams et al., 1962), and naturally, more cloudiness at
361 these five sites compared to the other sites located at lower elevation within/near the basins. This

362 is consistent with the significant negative correlations between summertime O₃ and relative
363 humidity at CNTL, ROMO, WICA, and the reference site YELL (Table S5). Note that no
364 significant partial correlation was found between summertime O₃ and relative humidity at GTHC,
365 indicating that summertime O₃ at this site was mostly influenced by wildfire emissions. Significant
366 correlations were also found between solar radiation and summertime median DM8HA O₃ at
367 CNTL ($r = 0.67, p = 0.05$), ROMO ($r = 0.43, p = 0.09$), WICA ($r = 0.62, p = 0.05$), and YELL (r
368 $= 0.72, p = 0.01$). These results indicate that reduced solar radiation flux near the surface resulting
369 from increased cloudiness accompanying increased precipitation resulted in less O₃ production
370 over the mountain ranges.

371 Situated on the southern section of the Black Hills, WICA received the highest summertime
372 average precipitation of 0.27 kg m⁻² (Figure 6a). Total Precipitation showed a significant negative
373 correlation with summertime median DM8HA O₃ at WICA ($r = -0.65, p = 0.04$, Figure 6b). As
374 noted in Section S5, the decadal highest summertime median DM8HA O₃ was observed in 2012
375 at 7 sites because of the decadal maximum wild fire emissions. WICA was the exception with its
376 2012 summertime median DM8HA O₃ being the second largest (58 ppbv) of the decade, compared
377 to the largest value of 61 ppbv in 2006 (Figure 3b), despite the fact that the decadal maximum total
378 fire index occurred in 2012 (0.022 g NO_x m⁻³ in Figure 6b). O₃ levels were expected to be lower
379 in the summer of 2006 because it had the least influence of wildfire emissions evidenced by a very
380 low total fire index value (0.010 g NO_x m⁻³) (Figure 6b). However, the decadal minimum
381 precipitation (0.18 kg m⁻²) in the summer of 2006 counteracted the effect of less wildfire emissions
382 (Figure 6b). By comparison, increased cloudiness accompanied more precipitation (0.22 kg m⁻²)
383 at WICA during the summer of 2012, which dominated over the influence of the decadal maximum
384 wildfire emissions (TFI = 0.021 g NO_x m⁻³). An increasing trend of 6.7 g m⁻² yr⁻¹ ($p = 0.17$) was

385 found in total precipitation at WICA for the time period of 2005 – 2015, indicative of increasing
386 cloudiness. Also, the A4DM8HA values at WICA occurred consistently in late spring/summer,
387 and ultimately the increasing trend in cloudiness linked to increased precipitation likely
388 contributed to the decreasing trend in the A4DM8HA over the decade at this site as shown in the
389 previous section.

390 Compared to YELL, CNTL, GTHC, ROMO, and WICA, sites located at the lower parts of
391 the basins (i.e., CANY, DINO, MEEK, RANG) had lower annual precipitation levels ranging from
392 0.08 – 0.12 kg m⁻² over 2005 – 2015 (Figure 6a). Significant negative correlations were only found
393 between summertime 5th percentile DM8HA O₃ and relative humidity at CANY, MEEK, RANG
394 (Table S5). This indicates that cloudiness associated with precipitation weather had a stronger
395 impact on summertime baseline O₃ than high percentile levels at sites within the basins.

396 **6. Contributions of transport from the Arctic and the West Coast and stratospheric intrusion** 397 **in winter**

398 Winter seasonal median DM8HA O₃ showed consistent interannual variation with higher O₃
399 levels (38 – 59 ppbv) in 2011 and 2013 whereas lower values (32 – 44 ppbv) in 2012 at the two
400 reference sites and most sites near/within O&NG basins, except the three high-elevation sites
401 ~~(i.e., GTHC, ROMO, and CNTL)~~ (Figures 3c-d). Seasonal 5th and 95th percentile values exhibited
402 similar patterns (not shown). Site and seasonal average O₃ mixing ratios exceeded the decadal
403 average 41 ppbv in 2006, 2008, 2010, 2011, and 2013, and were below average in 2007, 2009,
404 2012, 2014, and 2015. The difference of the 850 hPa geopotential height between the higher and
405 lower O₃ years is shown in Figure ~~6a~~7a. A pronounced positive difference of ~60 geopotential
406 meters (gpm) was observed over the Arctic polar region and a negative difference of ~ 40 gpm

407 over the midlatitudes. This pattern ~~strongly~~ indicates a negative (positive) phase of Arctic
408 Oscillation (AO) associated with a higher (lower) O₃ winter in the Intermountain West.

409 Indeed significant negative correlations (-0.91 to -0.58) were found between the AO index
410 and winter seasonal 50th/95th percentile DM8HA O₃ at most sites, including the reference site
411 YELL over 2005 – 2015 (Table ~~4~~2 and Figure ~~6b~~7b). Significant correlation was not found at the
412 other reference site CRMO, which is located to the south of the Pioneer Mountains and hardly
413 received ~~few~~ air masses (3%) from the north (Figure S1b). Weaker correlations were also observed
414 in the seasonal median DM8HA at CNTL and PNDE. During a longer time period dating back to
415 years prior to 2005, significant negative correlation was observed between seasonal median
416 DM8HA O₃ and the AO index at the reference site YELL (-0.45 over 1997 – ~~2005~~2015), as well
417 as at CANY (-0.47 over 1993 – 2015), CNTL (-0.46 over 1990 – 2015), and ROMO (-0.67 over
418 1988 – 2015). This ~~indicates~~suggests that the impact of AO on wintertime surface O₃ has been
419 consistently significant during different time periods over the past decades in the Intermountain
420 West.

421 The negative correlation between AO and wintertime O₃ could be a result of multiple
422 factors, including transport from the Arctic and California, in situ O₃ photochemical production,
423 and stratospheric intrusion. While long-term O₃ trends in lower percentiles could be influenced by
424 long-range transport, O₃ in higher percentiles was more sensitive to local emissions and extreme
425 events (Lin et al., 2017). First, the influence of transport from the Arctic was examined. Arctic
426 influence would be foremost demonstrated in surface temperature. During negative AO years,
427 frigid winter air masses could extend far into the middle of North America, contributing to
428 relatively cold temperatures over the U.S. Intermountain West (Hess and Lamarque, 2007).
429 Significant positive correlation was found between the AO index and surface temperature at

430 CANY, DINO, MEEK, RANG, and GTHC. Except for GTHC, all sites are located within the
431 basins, and weaker positive correlations were observed at other sites, except for CNTL, the highest
432 elevation site in this study (3175 m amsl) (Table Tables 1 and S1–2). Significant negative
433 correlation was also found between surface temperature and wintertime O₃ at sites within the basin
434 (i.e., CANY, DINO, MEEK, and RANG), with the potential effect of stratospheric intrusion
435 removed (Partial correlation in Table 42). Higher correlation coefficients were found in seasonal
436 50th/95th DM8HA at DINO, MEEK, and RANG, indicating that the sites were more likely under
437 local influence (Table 42). During a colder winter with constant snow cover, high concentrations
438 of O₃ precursors emitted from O&NG extraction were trapped in a shallow boundary layer within
439 the basins followed by strong O₃ photochemical production during daytime leading to the highest
440 O₃ mixing ratios of the season (Schnell et al., 2009; Edwards et al., 2014).

441 For sites outside the basins that are exposed to distant sources (Figure S1), the significant
442 correlation between wintertime median DM8HA O₃ and the AO index is a strong indication of
443 impacts of long-range transport from source regions afar.

444 Backward trajectory simulations suggest that long distance transport from the West Coast
445 may obscure the correlation between the AO index and surface O₃ at MEVE, ROMO, YELL,
446 WICA, CNTL, and PNDE. A total of 902 five-day backward trajectories were performed at each
447 site during winters of 2006 – 2015 (Figure 78). The difference in numbers of trajectories between
448 high and low O₃ years suggests that more air masses reached the six sites coming from low
449 altitudes (<900 hPa) over the area of southern California and Arizona, centered around
450 32.5 °N/120 °W during high O₃ years (Figure 78). At YELL, WICA, PNDE, ROMO, and CNTL,
451 more than 80 backward trajectories passed through the surface of California (Figure 78), where
452 ~~large amounts of abundant~~ O₃ could be produced from urban emissions ~~of facilities in urban areas~~

453 (Ryerson et al., 2013). Huang et al. (2013) also found that anthropogenic emissions from
454 southern California could contribute 1 – 15 ppbv to surface O₃ in air masses transported to the
455 Intermountain West. Additionally, more than 20 trajectories originating at YELL, CNTL,
456 ROMO, and MEVE came from higher altitudes (>700 hPa) in the north (>45 °N) during high O₃
457 years (Figure 78). During negative AO (high O₃) years, cold Arctic mid-tropospheric air rich in
458 O₃ would ~~cross Canada~~ reach midlatitudes more frequently (Mao and Talbot, 2004) including
459 the U.S. Intermountain West more frequently ((Hess and Lamarque, 2007)-) enhancing surface O₃
460 there. This is in part evidenced in the significant negative correlation ($r = -0.49, p = 0.01$) between
461 the AO index and lower tropospheric O₃ at Edmonton, Alberta, Canada over 1988 – 2014 (Figure
462 S2S3), indicating stronger impacts of Arctic mid-tropospheric O₃ on the Intermountain West
463 during negative AO years. This also contributes to explaining why the reference site YELL
464 experienced higher seasonal median DM8HA O₃.

465 Stratospheric influence on surface O₃ was also examined. One of the physical
466 characteristics of stratospheric air is high values of potential vorticity (~~PV~~). The differences in
467 ~~PV~~ potential vorticity between high and low O₃ years exhibited positive anomalies of ~ 0.5 ~~PV~~
468 ($10 \times 10^{-6} \text{ m}^2 \text{ s}^{-1} \text{ kg}^{-1} \text{ K}$) in the mid-troposphere (315 K) over the Intermountain West (Figure 89).
469 Significant negative correlations of -0.64 ($p < 0.01$) over 1988 – 2015 and -0.76 ($p = 0.01$) over
470 2005 – 2015 were found between PV and the AO index over the study region (37.5 °N – 45 °N, -
471 102.5 °W – -110°W). This indicated that stratospheric intrusion over the Intermountain West
472 was associated with the negative AO with a strong impact at on sites outside the basins over the
473 region.

474 **6. Effects of precipitation weather on summertime O₃**——

475 We found that summertime O_3 in the Intermountain West was strongly correlated with
476 relative humidity and the wildfire index total fire index (TFI) (Table S6). Studies have suggested
477 that in the Intermountain West, summertime O_3 , especially the seasonal high percentile levels, was
478 impacted by photochemical production from wildfire emissions (Table S6; Jaffe and Wigder, 2012;
479 Lu et al., 2016). To avoid repeating the extensive body of literature on this topic, our own analysis
480 of the effect of wildfires on O_3 can be found in Section S7. One key point coming out of our
481 analysis was, with fire influence removed as indicated in partial correlation, significant negative
482 correlations between summertime O_3 and relative humidity were found at the two reference sites
483 (CRMO and YELL), as well as at the 7 O&NG emission influenced sites (CANY CAMP, MEEK,
484 RANG, ROMO, PNDE, and WICA) (Table S6). Further investigation, detailed as follows,
485 revealed that this correlation essentially illuminated the effect of reduced solar radiation on O_3
486 production caused by cloudiness associated with precipitation weather.

487 In the Intermountain West, precipitation varies by elevation and latitude among other
488 factors (Williams et al., 1962). The decadal summertime average precipitation abundance was 0.17
489 $kg\ m^{-2}$ for the reference site YELL and 0.15 – $0.27\ kg\ m^{-2}$ for GTHC, CNTL, ROMO, and WICA,
490 which were higher than that at CRMO ($0.08\ kg\ m^{-2}$) and the remaining sites (Figure 9a). YELL,
491 GTHC, CNTL, ROMO, and WICA are located in the mountains, where localized convective
492 storms could develop quickly in summer leading to higher precipitation amounts (Williams et al.,
493 1962) and naturally, more cloudiness at these five sites compared to the other sites located within
494 the basins. This is consistent with the significant negative correlations between summertime O_3
495 and relative humidity at CNTL, ROMO, WICA, and the reference site YELL (Table S6). Note that
496 no significant partial correlation was found between summertime O_3 and relative humidity at
497 GTHC, indicating that summertime O_3 at this site was mostly influenced by wildfire emissions.

498 ~~Significant correlations were also found between solar radiation and summertime median DM8HA~~
499 ~~O_3 at CNTL ($r = 0.67$, $p = 0.05$), ROMO ($r = 0.43$, $p = 0.09$), WICA ($r = 0.62$, $p = 0.05$), and~~
500 ~~YELL ($r = 0.72$, $p = 0.01$). These results indicate that reduced solar radiation flux near the surface~~
501 ~~resulting from increased cloudiness accompanying increased precipitation resulted in less O_3~~
502 ~~production over the mountain ranges.~~

503 ~~Situated on the southern section of the Black Hills, WICA received the highest summertime~~
504 ~~average precipitation of 0.27 kg m^{-2} (Figure 9a). Total Precipitation showed a significant negative~~
505 ~~correlation with summertime median DM8HA O_3 at WICA ($r = -0.65$, $p = 0.04$, Figure 9b). As~~
506 ~~noted in Section S7, the decadal highest summertime median DM8HA O_3 was observed in 2012~~
507 ~~at 7 sites because of the decadal maximum wild fire emissions. WICA was the exception with its~~
508 ~~2012 summertime median DM8HA O_3 being the second largest (58 ppbv) of the decade, compared~~
509 ~~to the largest value of 61 ppbv in 2006 (Figure 3b), despite the fact that the decadal maximum TFI~~
510 ~~occurred in 2012 ($0.022 \text{ g NO}_x \text{ m}^{-3}$ in Figure 9b). O_3 levels were expected to be lower in the~~
511 ~~summer of 2006 because it had the least influence of wildfire emissions evidenced by a very low~~
512 ~~TFI value ($0.010 \text{ g NO}_x \text{ m}^{-3}$) (Figure 9b). However, the decadal minimum precipitation (0.18 kg~~
513 ~~m^{-2}) in the summer of 2006 counteracted the effect of less wildfire emissions (Figure 9b). By~~
514 ~~comparison, increased cloudiness accompanied more precipitation (0.22 kg m^{-2}) at WICA during~~
515 ~~the summer of 2012, which dominated over the influence of the decadal maximum wildfire~~
516 ~~emissions (TFI = $0.021 \text{ g NO}_x \text{ m}^{-3}$). An increasing trend of $6.7 \text{ g m}^{-2} \text{ yr}^{-1}$ ($p = 0.17$) was found in~~
517 ~~total precipitation at WICA for the time period of 2005–2015, indicative of increasing cloudiness~~
518 ~~and ultimately contributing to the decreasing trend in the A4DM8HA over the decade at this site.~~

519 ~~Compared to YELL, CNTL, GTHC, ROMO, and WICA, sites located at the lower parts of~~
520 ~~the basins (i.e., CANY, DINO, MEEK, RANG) had lower annual precipitation levels ranging from~~

521 ~~0.08 – 0.12 kg m⁻² over 2005 – 2015 (Figure 9a). Significant negative correlations were only found~~
522 ~~between summertime 5th percentile DM8HA O₃ and relative humidity at CANY, MEEK, RANG~~
523 ~~(Table S6). This indicates a stronger impact of cloudiness associated with precipitation weather on~~
524 ~~summertime baseline O₃ levels at sites within the basins.~~

525 **7. In situ photochemical O₃ production in winter and summer**

526 To determine the influence of in situ photochemical O₃ production on ambient O₃ in/near
527 O&NG basins, box model simulations were conducted for the Uintah-Piceance Basin, Denver-
528 Julesburg Basin, and its downwind region. In particular, field measurements of VOCs and NO_x in
529 the Uintah Basin during UBWOS 2012 – 2014 were used to understand the role of in situ
530 photochemistry in determining observed O₃ at RANG, DINO, and MEEK during winters of 2012
531 – 2014 (Figure 1). Measurements during FRAPPÉ at ROMO were used to determine
532 photochemically produced O₃ in summer 2014, while the NACHTT campaign at the Boulder
533 Atmospheric Observatory (BAO) Tower was used for winter 2011. Constraining the model
534 concentrations of VOCs, NO_x, and the radical precursors HCHO, HONO, and ClNO₂ using the
535 observed diel profiles reduced the impact of turbulent mixing and transport processes on the in situ
536 photochemical O₃ production. Details of the model simulations can be found in Section S8; Here
537 we focused on discussing the model results in the decadal context. Figure 10 compares the
538 observed average diel cycle of O₃ mixing ratios with those simulated for each campaign.
539 Differences between observed and simulated diel O₃ profiles represent the combined impact of
540 transport processes, stratospheric intrusion, and model uncertainty on surface O₃.

541 During NACHTT, photochemically produced O₃ at BAO ranged from 6 ppbv at 6:00 am MST
542 to 22 ppbv at 15:00 pm MST, contributing 20 – 52% of the observed O₃ (Figure 10a).
543 Photochemically produced O₃ contributed 30 – 60% of observed O₃ during UBWOS 2012 (Figure

544 10b). As seen in Figures 10c and 10d, it is possible for the contribution of photochemically
545 produced O₃ during UBWOS 2013 and UBWOS 2014 to exceed the observations. For example, a
546 modeled maximum value of 111 ppbv photochemically produced O₃ was simulated for 16:00 pm
547 MST during UBWOS 2013, larger than the 96 ppbv observed at the site, which indicates that
548 instantaneous mixing with surrounding air and fast transport lowered the photochemically
549 produced O₃ to the observed level.

550 The decadal highest winter seasonal median DM8HA O₃ was found at DINO (59 ppbv),
551 MEEK (44 ppbv), and RANG (44 ppbv) in winter 2013 (Figure 3c). A positive AO phase ~~was~~
552 ~~encountered during the~~occurred in winter ~~of~~ 2012 (Figure ~~5b6b~~), where ~~the ambient atmospheric~~
553 conditions were relatively warm without snow cover (Edwards et al., 2013), ~~and the resulting~~
554 ~~conditions exhibited only~~leading to moderate O₃ production (~31 ppbv in Figure 10b). In contrast
555 to 2012, winter 2013 was in a negative AO phase (Figure ~~6b7b~~), placing the Intermountain West
556 under a strong influence of frigid Arctic air (Section ~~56~~) and subsequently under meteorologically
557 stagnant conditions and increased snow cover within the basins. As a result, the high levels of
558 VOC emissions from O&NG fields ~~that~~ accumulated in the shallow boundary layer coupled with
559 the increased photolysis rates ~~from the~~due to snow albedo contributed to rapid O₃ production (~78
560 ppbv in Figure 10c) within the basin, consistent with results from Edward et al. (2014). This result
561 supports the point that surface O₃ at the sites within the basins was attributed mostly to in situ
562 photochemical reactions (Section ~~56~~).

563 In contrast to the four wintertime campaigns described above, FRAPPÉ was conducted in
564 the summer. The O₃ measurements from ROMO, located in the center of the FRAPPÉ campaign
565 area, showed a diel cycle with ~40 ppbv nighttime and ~49 ppbv daytime O₃ levels. In contrast,
566 photochemically produced O₃ at ROMO showed a distinct diel cycle with 0 ppbv at night and ~41

567 ppbv during the day. The strong diel cycle of photochemical production of O₃ at ROMO probably
568 resulted from the combined effect of its high elevation and close proximity to the NFR-Colorado
569 Northern Front Range. During the day, large amounts of O₃ precursors from the NFRColorado
570 Northern Front Range transported upward from the southeast (Figure 5a) and contributed to
571 photochemical O₃ production at ROMO (Benedict et al., 2018) followed by dramatically decreased
572 photochemical production accompanied by the collapse of the planetary boundary layer during
573 sunset at ~20:00 MST.

574 **7.1 VOCs-NO_x-O₃ sensitivity**

575 The O₃ sensitivity to NO_x and VOC emissions, which is relevant to the attainment of
576 regional air quality standards, was evaluated in/near O&NG basins. Fifteen simulations for each
577 field campaign were performed with sealed-observed VOC and NO_x mixing ratios-and, the base
578 case-VOC scenario latter (NO_x) of which were scaled by a factor varying from 0 to test the
579 sensitivity of daily maximum photochemical O₃ production-5. NO_x scaling factor of 1 indicates
580 observed NO_x mixing ratios (Figure 10f). The O₃ formation regime was found be closely
581 associated to with the AO phase. Photochemically produced O₃ during UBWOS 2012 and UBWOS
582 2014 was sensitive to VOCs (Figure 10f),decreased with increasing NO_x mixing ratios, indicating
583 thatVOC-limited O₃ formation regimes (Figure 10f). Therefore, O₃ photochemistry at DINO,
584 RANG, and MEEK was also likely to be radical limited in winter 2012 and 2014. In contrast to
585 these two winters, O₃ photochemistry had mixed sensitivity during UBWOS 2013 (Figure 10f),
586 when in situ photochemically produced O₃ could be as high as 111 ppbv. Winter 2013 was in a
587 negative AO phase, while winters of 2012 and 2014 were in positive phases. As stated in Section
588 5aforementioned, surface O₃ at the sites within the basin was attributed mostly to in situ
589 photochemical reactions. Therefore, for areas within the basins, emission reductions in VOCs

590 alone would lead to O₃ mitigation in positive AO years, while emission reductions in both VOCs
591 and NO_x would be effective in negative AO years. In the NFRColorado Northern Front Range
592 region, photochemical O₃ production in winter 2011 surrounding BAO was sensitive to VOCs
593 during NACHTT (Figure 10f). Photochemical O₃ production at ROMO in summer 2014 had mixed
594 sensitivity (Figure 10f).

595 Edwards et al. (2013) also simulated an average UBWOS 2012 day (15 January to 1 March
596 2012) and found the same O₃ formation regime as our study. They found that the radical-limited
597 O₃ photochemistry in 2012 was driven by the very low radical production rates (~2.3 ppbv day⁻¹)
598 in comparison to the emission rate of NO_x. While an average UBWOS 2013 day (23 January to 24
599 March 2013) was simulated in our study, Edwards et al. (2014) simulated a single stagnant six-
600 day (31 January to 5 February 2013) stronghigh O₃ event, when DM8HA O₃ increased from 67 to
601 107 ppbv. ~~It was~~They found that O₃ in winter 2013 was sensitive to changes of NO_x, and the total
602 net radical production rate could be as high as ~19 ppbv day⁻¹, which was sufficient to prevent
603 NO_x saturation (~~Edward et al., 2014~~).

604 **8. Summary**

605 ~~Our study suggested that decadal~~Two reference sites, YELL and CRMO, exhibited no
606 significant trends in the A4DM8HA O₃ over ~~the Intermountain West during~~ 2005 – 2015. Our
607 analysis suggested that, without the immediate influence of O&NG emissions, the lack of trend
608 and the interannual variation at the two reference sites were ~~shaped~~driven by precipitation weather,
609 wildfire emissions, stratospheric intrusion, and transport from the Arctic and the West Coast
610 facilitated by regional to hemispheric circulation. ~~Trends over the areas~~In contrast, decadal trends
611 at sites near/within O&NG basins were predominantly impacted by changes in emissions from the
612 O&NG basins among other anthropogenic sources. ~~Two reference sites, YELL and CRMO,~~

613 ~~exhibited no significant trends in the A4DM8HA O₃ over 2005–2015, indicating, without the~~
614 ~~immediate influence of O&NG emissions, relatively constant O₃ levels over the Intermountain~~
615 ~~West. In contrast, decadal trends in the A4DM8HA varied at the 11 sites located either in or near~~
616 ~~the O&NG extraction basins. A significant decreasing trend of -0.76~~ A significant decreasing trend
617 of -0.83 ppbv yr⁻¹ at MEVE was associated with the decreasing natural gas production (37%) in
618 the San Juan Basin, while ~~a significant decreasing trend (that of -0.5458~~ ppbv yr⁻¹) at CANY was
619 predominately influenced by declining extraction of CBM in the Paradox Basin and emission
620 reductions of 35% in electricity generation from coal. Increasing precipitation (6.7 g m⁻² yr⁻¹)
621 resulting from increasing cloudiness ~~in the southern portion of the Black Hills~~ contributed to the
622 decreasing trend in the A4DM8HA (-1.2416 ppbv yr⁻¹) at WICA. No trends were found ~~in the~~
623 ~~4DM8HA~~ at the remaining sites, resulting likely from the combined effect of increasing emissions
624 from O&NG extraction and decreasing emissions from other sectors.

625 In winter, seasonal 50th/95th DM8HA O₃ was associated with the AO at 8 sites, including
626 the reference site YELL. For sites within the O&NG basins, O&NG emissions, colder surface air
627 temperature, and enhanced solar radiation due to snow cover contributed to higher O₃, especially
628 in the seasonal 95th levels during negative AO years, and emission reductions in both VOCs and
629 NO_x could lead to effective O₃ mitigation. For sites outside the O&NG basins, the ~~high O₃ in~~ higher
630 seasonal 50th percentile DM8HA O₃ levels were a result of transport from the Arctic or California
631 ~~and~~ together with stratospheric intrusion. In summer, the interannual variation of O₃ was
632 predominantly affected by precipitation weather at 9 sites including the two reference sites. At
633 high-elevation sites in the mountains, more abundant precipitation (0.18 – 0.27 kg m⁻²) induced
634 more cloudiness and consequently reduced solar flux leading less O₃ production in seasonal
635 5th/50th/95th levels. However, at sites within the basin, the cloudiness associated with precipitation

636 weather had a stronger impact on summertime baseline O₃ levels (i.e., the 5th percentile).

637 ~~This study is the first one to investigate the long-term impact of O&NG extraction activities~~
638 ~~on the distribution and trend of surface O₃ over the intermountain U.S. To the best of our knowledge,~~
639 ~~only two studies investigated the long-term impact of O&NG extraction on the trend of surface O₃~~
640 ~~and its precursors (Majid et al., 2017; Bien and Helmig, 2018). Majid et al. (2017) investigated the~~
641 ~~decadal trends in OMI-retrieved NO₂ in 7 main shale plays over 2005 – 2015 and found O&NG~~
642 ~~industry was reversing the rate of changes in NO₂. Bien and Helmig (2018) found surface O₃ at~~
643 ~~sites within O&NG production basins can be ranked among top ten of all Colorado sites, and~~
644 ~~further suggested the need of more continuous measurements within O&NG basins to study the~~
645 ~~long-term influence of O&NG emissions.~~ O&NG activities have varied greatly over the past
646 decade. In Wyoming, annual O&NG production levels have fallen significantly in the Jonah Field
647 since 2009 and the Pinedale Field since 2012, because of lower natural gas prices relative to crude
648 oil (<http://wogcc.wyo.gov/>). In Colorado, the number of active wells in Weld County increased by
649 ~2000 between 2012 and 2014, followed by a decline since early 2015
650 (<http://cogcc.state.co.us/data.html>). However, current emission inventories underestimated VOC
651 emissions from O&NG productions by a factor of 2 or more (Péron et al., 2014). While data
652 analysis studies provided measurement-based estimates of contributions from various processes to
653 decadal variability of surface O₃, we understand their limitation in clearly separating such
654 contributions. Detailed multiyear studies that integrate measurements and three-dimensional
655 chemical transport model simulations with accurate emission inventories are needed to further
656 quantify the contribution of each process identified in this work.

657 **Author Contributions**

658 YZ and HM designed this study. BS provided long-term surface observations. YZ led the analysis

659 and writing of this manuscript ~~with~~, HM contributed to manuscript writing, and BS contributed
660 significant ~~contributions~~scientific and editorial comments ~~from HM and BS~~.

661 **Acknowledgements**

662 This work was supported by the Chemistry Emeriti Faculty Award from the Department of
663 Chemistry at SUNY College of Environmental Science and Forestry and the National Park Service.

664 We are grateful to Jessica Ward, Air Resources Specialists, Inc. for retrieving and providing the
665 National Park Service data. We thank Cara Kesler for providing data from the Wyoming

666 Department of Environmental Quality. We acknowledge the free use of tropospheric NO₂ column
667 data from the OMI sensor from www.temis.nl. We thank the two anonymous reviewers for their

668 constructive comments and suggestions. The assumptions, findings, conclusions, judgements, and
669 views presented herein are those of the authors and should not be interpreted as necessarily

670 representing the National Park Service.

671 **References**

672 Abeleira, A. J. and Farmer, D. K.: Summer ozone in the northern Front Range metropolitan area:
673 weekend–weekday effects, temperature dependences, and the impact of drought. *Atmos. Chem.*
674 *Phys.*, 17, 6517-6529, <https://doi.org/10.5194/acp-17-6517-2017>, 2017.

675 Akagi, S. K., Yokelson, R. J., Wiedinmyer, C., Alvarado, M. J., Reid, J. S., Karl, T., Crounse, J.
676 D., and Wennberg, P. O.: Emission factors for open and domestic biomass burning for use in
677 atmospheric models. *Atmos. Chem. Phys.*, 11, 4039-4072, [https://doi.org/10.5194/acp-11-4039-](https://doi.org/10.5194/acp-11-4039-2011)
678 2011, 2011.

679 Allen, D.T.: Atmospheric emissions and air quality impacts from natural gas production and use,
680 *Annu. Rev. Chem. Biomol. Eng.* 5, 55-75, doi:10.1146/annurev-chembioeng-060713-035938,
681 2014.

682 Allen, D. T.: Emissions from oil and gas operations in the United States and their air quality
683 implications, *Journal of the Air & Waste Management Association*, 66:6,549-575, DOI:
684 10.1080/10962247.2016.1171263, 2016.

685 Benedict, K. B., Zhou, Y., Sive, B. C., Prenni, A. J., Gebhart, K. A., Fischer, E. V., Evanski-Cole,
686 A., Sullivan, A. P., Callahan, S., Schichtel, B. A., Mao, H., Zhou, Y., and Collett Jr., J. L.: Volatile
687 organic compounds and ozone in Rocky Mountain National Park during FRAPPÉ, *Atmos. Chem.*
688 *Phys.*, 19, 499-521, <https://doi.org/10.5194/acp-19-499-2019>, 2019.

689 Bien, T. and Helmig, D.: Changes in summertime ozone in Colorado during 2000–2015. *Elem Sci*

690 [Anth, 6\(1\), p.55. DOI: http://doi.org/10.1525/elementa.300, 2018.](#)

691 Carter, W. P. L. and Seinfeld, J. H.: Winter ozone formation and VOC incremental reactivities in
692 the Upper Green River Basin of Wyoming. *Atmospheric Environment*, 50, 255-266,
693 <https://doi.org/10.1016/j.atmosenv.2011.12.025>, 2012

694 Chan, E.: Regional ground-level ozone trends in the context of meteorological influences across
695 Canada and the eastern United States from 1997 to 2006. *Journal of Geophysical Research:*
696 *Atmospheres*, 114, 1-18, <https://doi.org/10.1029/2008JD010090>, 2009.

697 [Cheadle, L.C., Oltmans, S.J., Petron, G., Schnell, R.C., Mattson, E.J., Herndon, S.C., Thompson,](#)
698 [A.M., Blake, D.R. and McClure-Begley, A., 2017. Surface ozone in the Colorado northern Front](#)
699 [Range and the influence of oil and gas development during FRAPPE/DISCOVER-AQ in summer](#)
700 [2014. Elem Sci Anth, 5, p.61. DOI: http://doi.org/10.1525/elementa.254](#)

701 Cooper, O. R., Gao, R. S., Tarasick, D., Leblanc, T., and Sweeney, C.: Long-term ozone trends at
702 rural ozone monitoring sites across the United States, 1990-2010. *Journal of Geophysical Research:*
703 *Atmospheres*, 117, 1990-2010, <https://doi.org/10.1029/2012JD018261>, 2012.

704 [Cooper, O.R., Parrish, D.D., Ziemke, J., Balashov, N.V., Cupeiro, M., Galbally, I.E., Gilge, S.,](#)
705 [Horowitz, L., Jensen, N.R., Lamarque, J.-F., Naik, V., Oltmans, S.J., Schwab, J., Shindell, D.T.,](#)
706 [Thompson, A.M., Thouret, V., Wang, Y. and Zbinden, R.M.: Global distribution and trends of](#)
707 [tropospheric ozone: An observation-based review. Elem Sci Anth, 2, p.000029.](#)
708 [DOI:http://doi.org/10.12952/journal.elementa.000029, 2014.](#)

709 Draxler, R. R., and Hess, G. D.: NOAA Technical Memorandum ERL ARL-224, 28.
710 <https://www.arl.noaa.gov/documents/reports/arl-224.pdf>, 1998.

711 Edwards, P. M., Young, C. J., Aikin, K., deGouw, J., Dubé W. P., Geiger, F., Gilman, J., Helmig,
712 D., Holloway, J. S., Kercher, J., Lerner, B., Martin, R., McLaren, R., Parrish, D. D., Peischl, J.,
713 Roberts, J. M., Ryerson, T. B., Thornton, J., Warneke, C., Williams, E. J., and Brown, S. S.: Ozone
714 photochemistry in an oil and natural gas extraction region during winter: simulations of a snow-
715 free season in the Uintah Basin, Utah, *Atmos. Chem. Phys.*, 13, 8955-8971,
716 <https://doi.org/10.5194/acp-13-8955-2013>, 2013.

717 Edwards, P.M., Brown, S.S., Roberts, J.M., Ahmadov, R., Banta, R.M., DeGouw, J. A., Dubé
718 W.P., Field, R. A., Flynn, J.H., Gilman, J.B., Graus, M., Helmig, D., Koss, A., Langford, A.O.,
719 Lefer, B.L., Lerner, B.M., Li, R., Li, S.-M., McKeen, S. A., Murphy, S.M., Parrish, D.D., Senff,
720 C.J., Soltis, J., Stutz, J., Sweeney, C., Thompson, C.R., Trainer, M.K., Tsai, C., Veres, P.R.,
721 Washenfelder, R. a., Warneke, C., Wild, R.J., Young, C.J., Yuan, B., Zamora, R: High winter
722 ozone pollution from carbonyl photolysis in an oil and gas basin. *Nature*, 514(7522), 351-354,
723 <https://doi.org/10.1038/nature13767>, 2014.

724 Energy Information Administration (EIA): Shale in the United States. Retrieved from
725 http://www.eia.gov/energy_in_brief/article/shale_in_the_united_states.cfm, 2015.

726 Environmental Protection Agency (EPA): Regulatory Actions | Ground-level Ozone | US EPA.
727 Retrieved February 8, 2016, from <http://www3.epa.gov/ozonepollution/actions.html>, 2015.

728 Helmig, D., Thompson, C. R., Evans, J., Boylan, P., Hueber, J., and Park, J.-H.: Highly elevated
729 atmospheric levels of volatile organic compounds in the Uintah Basin, Utah. *Environmental*
730 *Science & Technology*, 48, 4707-4715, <https://doi.org/10.1021/es405046r>, 2014.

731 Gaudel, A., Cooper, O.R., Ancellet, G., Barret, B., Boynard, A., Burrows, J.P., Clerbaux, C.,
732 Coheur, P.-F., Cuesta, J., Cuevas, E., Doniki, S., Dufour, G., Ebojie, F., Foret, G., Garcia, O.,
733 Granados Muñoz, M.J., Hannigan, J.W., Hase, F., Huang, G., Hassler, B., Hurtmans, D., Jaffe, D.,
734 Jones, N., Kalabokas, P., Kerridge, B., Kulawik, S.S., Latter, B., Leblanc, T., Le Flochmoën, E.,
735 Lin, W., Liu, J., Liu, X., Mahieu, E., McClure-Begley, A., Neu, J.L., Osman, M., Palm, M., Petetin,
736 H., Petropavlovskikh, I., Querel, R., Rahpoe, N., Rozanov, A., Schultz, M.G., Schwab, J., Siddans,
737 R., Smale, D., Steinbacher, M., Tanimoto, H., Tarasick, D.W., Thouret, V., Thompson, A.M.,
738 Trickl, T., Weatherhead, E., Wespes, C., Worden, H.M., Vigouroux, C., Xu, X., Zeng, G. and
739 Ziemke, J.: Tropospheric Ozone Assessment Report: Present-day distribution and trends of
740 tropospheric ozone relevant to climate and global atmospheric chemistry model evaluation. *Elem*
741 *Sci Anth*, 6, p.39, <http://doi.org/10.1525/elementa.291>, 2018.

742 Hess, P. G. and Lamarque, J. F.: Ozone source attribution and its modulation by the Arctic
743 oscillation during the spring months. *Journal of Geophysical Research: Atmospheres*, 112, 1-17,
744 <https://doi.org/10.1029/2006JD007557>, 2007.

745 Huang, M., Bowman, K. W., Carmichael, G. R., Bradley, P. R., Worden, H. M., Luo, M., Cooper,
746 O. R., Pollack, I. B., Ryerson, T. B., Brown, S. S.: Impact of Southern California anthropogenic
747 emissions on ozone pollution in the mountain states: Model analysis and observational evidence
748 from space. *Journal of Geophysical Research: Atmospheres*, 118, 12,784-12,803,
749 <https://doi.org/10.1002/2013JD020205>, 2013.

750 Jaffe, D., Chand, D., Hafner, W., Westerling, A., and Spracklen, D.: Influence of Fires on O₃
751 Concentrations in the Western U.S. *Environmental Science & Technology*, 42, 5885-5891,
752 <https://doi.org/10.1021/es800084k>, 2008.

753 Jaffe, D. A. and Wigder, N. L.: Ozone production from wildfires: A critical review. *Atmospheric*
754 *Environment*, 51, 1-10, <https://doi.org/10.1016/j.atmosenv.2011.11.063>, 2012.

755 Jenkin, M. E., Young, J. C., and Rickard, A. R.: The MCM v3.3.1 degradation scheme for isoprene.
756 *Atmos. Chem. Phys.*, 15, 11433-11459, <https://doi.org/10.5194/acp-15-11433-2015>, 2015.

757 Karion, A., Sweeney, C., Petron, G., Frost, G., Hardesty, R. M., Kofler, J., Miller, B. R.,
758 Newberger, T., Wolter, S., Banta, R., Brewer, A., Dlugokencky, E., Lang, P., Montzka, S. A.,
759 Schnell, R., Tans, P., Trainer, M., Zamora, R., Conley, S.: Methane emissions estimate from
760 airborne measurements over a western United States natural gas field *Geophys. Res. Lett.*, 40,
761 4393-4397, DOI: 10.1002/grl.50811, 2013.

762 Knote, C., Tuccella, P., Curci, G., Emmons, L., Orlando, J.J., Madronich, S., Baró R., Jiménez-
763 Guerrero, P., Luecken, D., Hogrefe, C., Forkel, R., Werhahn, J., Hirtl, M., Pérez, J.L., San José
764 R., Giordano, L., Brunner, D., Yahya, K., Zhang, Y.: Influence of the choice of gas-phase
765 mechanism on predictions of key gaseous pollutants during the AQMEII phase-2 intercomparison.
766 *Atmospheric Environment*, 115, 553-568, <https://doi.org/10.1016/j.atmosenv.2014.11.066>, 2015.

767 Lin, M., Horowitz, L. W., Payton, R., Fiore, A. M., and Tonnesen, G.: US surface ozone trends
768 and extremes from 1980 to 2014: quantifying the roles of rising Asian emissions, domestic controls,
769 wildfires, and climate. *Atmos. Chem. Phys.*, 17, 2943-2970, [https://doi.org/10.5194/acp-17-2943-](https://doi.org/10.5194/acp-17-2943-2017)
770 2017, 2017.

771 Lin, M., Horowitz, L. W., Oltmans, S. J., Fiore, A. M., and Fan, S.: Tropospheric ozone trends at
772 Mauna Loa Observatory tied to decadal climate variability. *Nature Geoscience*, 7, 136-143,
773 <https://doi.org/10.1038/ngeo2066>, 2014.

774 Lu, X., Zhang, L., Yue, X., Zhang, J., Jaffe, D. A., Stohl, A., Zhao, Y., and Shao, J.: Wildfire
775 influences on the variability and trend of summer surface ozone in the mountainous western United
776 States, *Atmos. Chem. Phys.*, 16, 14687-14702, <https://doi.org/10.5194/acp-16-14687-2016>, 2016.

777 Madronich, S., McKenzie, R. L., Björn, L. O., and Caldwell, M. M.: Changes in biologically active
778 ultraviolet radiation reaching the Earth's surface. *Journal of Photochemistry and Photobiology B:
779 Biology*, 46, 5-19, [https://doi.org/10.1016/S1011-1344\(98\)00182-1](https://doi.org/10.1016/S1011-1344(98)00182-1), 1998.

780 [Mao, H., and Talbot, R.: Relationship of surface O₃ to large-scale circulation patterns during two](#)
781 [recent winters, *Geophys. Res. Lett.*, 31\(6\), L06108, 10.1029/2003GL018860, 2004.](#)

782 Natural Gas Intelligence (NGI): Major & Minor Resource Plays. Retrieved April 27, 2018, from
783 [http://www.naturalgasintel.com/Major-and-Minor-North-American-Shale-Basins-and-Resource-](http://www.naturalgasintel.com/Major-and-Minor-North-American-Shale-Basins-and-Resource-Plays)
784 [Plays](http://www.naturalgasintel.com/Major-and-Minor-North-American-Shale-Basins-and-Resource-Plays), 2018.

785 McDuffie, E. E., Edwards, P. M., Gilman, J. B., Lerner, B. M., Dubé W. P., Trainer, M., Wolfe,
786 D. E., Angevine, W. M., deGouw, J., Williams, E. J., Tevlin, A. G., Murphy, J. G., Fischer, E. V.,
787 McKeen, S., Ryerson, T. B., Peischl, J., Holloway, J. S., Aikin, K., Langford, A. O., Senff, C. J.,
788 Alvarez, R. J., Hall, S. R., Ullmann, K., Lantz, K. O., Brown, S. S.: Influence of oil and gas
789 emissions on summertime ozone in the Colorado Northern Front Range. *Journal of Geophysical
790 Research: Atmospheres*, 121, 8712-8729, <https://doi.org/10.1002/2016JD025265>, 2016.

791 Monks, P.S., Granier, C., Fuzzi, S., Stohl, A., Williams, M.L., Akimoto, H., Amann, M., Baklanov,
792 A., Baltensperger, U., Bey, I., Blake, N., Blake, R.S., Carslaw, K., Cooper, O.R., Dentener, F.,
793 Fowler, D., Fragkou, E., Frost, G.J., Generoso, S., Ginoux, P., Grewe, V., Guenther, A., Hansson,
794 H.C., Henne, S., Hjorth, J., Hofzumahaus, A., Huntrieser, H., Isaksen, I.S.A., Jenkin, M.E., Kaiser,
795 J., Kanakidou, M., Klimont, Z., Kulmala, M., Laj, P., Lawrence, M.G., Lee, J.D., Liousse, C.,
796 Maione, M., McFiggans, G., Metzger, A., Mieville, A., Moussiopoulos, N., Orlando, J.J., O'Dowd,
797 C.D., Palmer, P.I., Parrish, D.D., Petzold, A., Platt, U., Pöschl, U., Prévôt, A.S.H., Reeves, C.E.,
798 Reimann, S., Rudich, Y., Sellegri, K., Steinbrecher, R., Simpson, D., ten Brink, H., Theloke, J.,
799 van der Werf, G.R., Vautard, R., Vestreng, V., Vlachokostas, C., von Glasow, R.: Atmospheric
800 composition change – global and regional air quality. *Atmospheric Environment*, 43, 5268-5350,
801 <https://doi.org/10.1016/j.atmosenv.2009.08.021>, 2009.

802 [Oltmans, S.J., Cheadle, L.C., Johnson, B.J., Schnell, R.C., Helmig, D., Thompson, A.M., Cullis,](#)
803 [P., Hall, E., Jordan, A., Sterling, C., McClure-Begley, A., Sullivan, J.T., McGee, T.J. and Wolfe,](#)
804 [D., 2019. Boundary layer ozone in the Northern Colorado Front Range in July–August 2014 during](#)
805 [FRAPPE and DISCOVER-AQ from vertical profile measurements. *Elem Sci Anth*, 7\(1\), p.6. DOI:](#)
806 <http://doi.org/10.1525/elementa.345>

807 Parrish, D.D., Law, K.S., Staehelin, J., Derwent, R., Cooper, O.R., Tanimoto, H., Volz-Thomas,
808 A., Gilge, S., Scheel, H.E., Steinbacher, M., Chan, E.: Long-term changes in lower tropospheric
809 baseline ozone concentrations at northern mid-latitudes. *Atmos. Chem. Phys.*, 12, 11485-11504,
810 <https://doi.org/10.5194/acp-12-11485-2012>, 2012.

811 Parrish, D.D., Law, K.S., Staehelin, J., Derwent, R., Cooper, O.R., Tanimoto, H., Volz-Thomas,
812 A., Gilge, S., Scheel, H.E., Steinbacher, M., Chan, E.: Lower tropospheric ozone at northern
813 midlatitudes: Changing seasonal cycle. *Geophysical Research Letters*, 40, 1631-1636,
814 <https://doi.org/10.1002/grl.50303>, 2013.

815 Páron, G., Karion, A., Sweeney, C., Miller, B.R., Montzka, S.A., Frost, G.J., Trainer, M., Tans,
816 P., Andrews, A., Kofler, J., Helmig, D., Guenther, D., Dlugokencky, E., Lang, P., Newberger, T.,

817 Wolter, S., Hall, B., Novelli, P., Brewer, A., Conley, S., Hardesty, M., Banta, R., White, A., Noone,
818 D., Wolfe, D., Schnell, R.: A new look at methane and nonmethane hydrocarbon emissions from
819 oil and natural gas operations in the Colorado Denver-Julesburg Basin. *Journal of Geophysical*
820 *Research: Atmospheres*, 119, 6836-6852, <https://doi.org/10.1002/2013JD021272>, 2014.

821 Pfister G. G., Reddy P. J., Barth M. C., Flocke F. F., Fried A., Herndon S. C., Sive B. C., Sullivan
822 J. T., Thompson A. M., Yacovitch T. I., Weinheimer A. J., Wisthaler A.: Using Observations and
823 Source - Specific Model Tracers to Characterize Pollutant Transport During FRAPPÉ and
824 DISCOVER - AQ. *Journal of Geophysical Research: Atmospheres*, 122, 10,510-10,538,
825 <https://doi.org/10.1002/2017JD027257>, 2007.

826 Rappenglück, B., Ackermann, L., Alvarez, S., Golovko, J., Buhr, M., Field, R. A., Soltis, J.,
827 Montague, D. C., Hauze, B., Adamson, S., Risch, D., Wilkerson, G., Bush, D., Stoeckenius, T.,
828 and Keslar, C.: Strong wintertime ozone events in the Upper Green River basin, Wyoming, *Atmos.*
829 *Chem. Phys.*, 14, 4909-4934, <https://doi.org/10.5194/acp-14-4909-2014>, 2014.

830 Reddy, P. J. and Pfister, G. G.: Meteorological factors contributing to the interannual variability
831 of midsummer surface ozone in Colorado, Utah, and other western U.S. states. *Journal of*
832 *Geophysical Research: Atmospheres*, 121, 2434-2456, <https://doi.org/10.1002/2015JD023840>,
833 2016.

834 Reidmiller, D. R., Fiore, A. M., Jaffe, D. A., Bergmann, D., Cuvelier, C., Dentener, F. J., Duncan,
835 B. N., Folberth, G., Gauss, M., Gong, S., Hess, P., Jonson, J. E., Keating, T., Lupu, A., Marmer,
836 E., Park, R., Schultz, M. G., Shindell, D. T., Szopa, S., Vivanco, M. G., Wild, O., and Zuber, A.:
837 The influence of foreign vs. North American emissions on surface ozone in the US, *Atmos. Chem.*
838 *Phys.*, 9, 5027-5042, <https://doi.org/10.5194/acp-9-5027-2009>, 2009.

839 Rodriguez, M. A., Barna, M. G., and Moore, T.: Regional Impacts of Oil and Gas Development
840 on Ozone Formation in the Western United States. *Journal of the Air & Waste Management*
841 *Association*, 59, 1111-1118, <https://doi.org/10.3155/1047-3289.59.9.1111>, 2009.

842 Ryerson T. B., Andrews A. E., Angevine W. M., Bates T. S., Brock C. A., Cairns B., Cohen R. C.,
843 Cooper O. R., Gouw J. A., Fehsenfeld F. C., Ferrare R. A., Fischer M. L., Flagan R. C., Goldstein
844 A. H., Hair J. W., Hardesty R. M., Hostetler C. A., Jimenez J. L., Langford A. O., McCauley E.,
845 McKeen S. A., Molina L. T., Nenes A., Oltmans S. J., Parrish D. D., Pederson J. R., Pierce R. B.,
846 Prather K., Quinn P. K., Seinfeld J. H., Senff C. J., Sorooshian A., Stutz J., Surratt J. D., Trainer
847 M., Volkamer R., Williams E. J., Wofsy S. C.: The 2010 California Research at the Nexus of Air
848 Quality and Climate Change (CalNex) field study. *Journal of Geophysical Research: Atmospheres*,
849 118, 5830-5866, <https://doi.org/10.1002/jgrd.50331>, 2013.

850 Schnell, R. C., Oltmans, S. J., Neely, R. R., Endres, M. S., Molenaar, J. V., and White, A. B.: Rapid
851 photochemical production of ozone at high concentrations in a rural site during winter. *Nature*
852 *Geoscience*, 2, 120-122, <https://doi.org/10.1038/ngeo415>, 2009.

853 Stohl A., Bonasoni P., Cristofanelli P., Collins W., Feichter J., Frank A., Forster C., Gerasopoulos
854 E., Gäggeler H., James P., Kentarchos T., Kromp-Kolb H., Krüger B., Land C., Meloan J.,
855 Papayannis A., Priller A., Seibert P., Sprenger M., Roelofs G. J., Scheel H. E., Schnabel C.,
856 Siegmund P., Tobler L., Trickl T., Wernli H., Wirth V., Zanis P., Zerefos C.: Stratosphere -
857 troposphere exchange: A review, and what we have learned from STACCATO. *Journal of*
858 *Geophysical Research: Atmospheres*, 108, <https://doi.org/10.1029/2002JD002490>, 2003.

859 Swarthout, R. F., Russo, R. S., Zhou, Y., Hart, A. H., and Sive, B. C.: Volatile organic compound
860 distributions during the NACHTT campaign at the Boulder Atmospheric Observatory: Influence
861 of urban and natural gas sources. *Journal of Geophysical Research: Atmospheres*, 118, 10,614-
862 10,637, <https://doi.org/10.1002/jgrd.50722>, 2013.

863 Thompson, T. M., D. Shepherd, A. Stacy, M. G. Barna, and B. A. Schichtel: Modeling to Evaluate
864 Contribution of Oil and Gas Emissions to Air Pollution, *Journal of the Air & Waste Management*
865 *Association*, 67, 445-461, DOI:10.1080/10962247.2016.1251508, 2017.

866 Westerling, A. L., Hidalgo, H. G., Cayan, D. R., and Swetnam, T. W.: Warming and Earlier Spring
867 Increase Western U.S. Forest Wildfire Activity. *Science*, 313, 940-943,
868 <https://doi.org/10.1126/science.1128834>, 2006.

869 Williams, P. and Peck, E. L.: Terrain Influences on Precipitation in the Intermountain West as
870 Related to Synoptic Situations. *Journal of Applied Meteorology*, 1, 343-347,
871 [https://doi.org/10.1175/1520-0450\(1962\)001<0343:TIOFIT>2.0.CO;2](https://doi.org/10.1175/1520-0450(1962)001<0343:TIOFIT>2.0.CO;2), 1962.

872 Zhou, Y., Mao, H., Demerjian, K., Hogrefe, C., and Liu, J.: Regional and hemispheric influences
873 on temporal variability in baseline carbon monoxide and ozone over the Northeast US.
874 *Atmospheric Environment*, 164, 309-324, <https://doi.org/10.1016/j.atmosenv.2017.06.017>, 2017.

875

876

877

878

879

880

881

882

883

884

885

886

887

888

889

890

891

892 Table 1. Names and locations of sites used in this study. Gray and blue shades indicate sites located outside of 100 km of shale plays. CRMO and YELL in blue
 893 shades are located upwind of O&NG extraction fields and used as reference sites.

894

Site Abbreviation	Park Unit/Measurement Network	Site	Latitude	Longitude	Elevation (m)	Start Date	End Date	Year-round Measurement
CANY	Canyonlands National Park	Island in the Sky	38.46	-109.82	1809	7/1/1992	12/30/2015	1993 - 2015
DINO	Dinosaur National Monument	West Entrance Housing	40.29	-108.94	1463	4/1/2005	12/30/2015	2011 - 2015
MEEK	Meeker	Plant Science Resource Management	40.00	-107.85	1994	1/1/2010	12/30/2015	2010 - 2015
MEVE	Mesa Verde National Park	Area	37.20	-108.49	2165	3/1/1993	12/30/2015	1995 - 2015
RANG	Rangely	Golf Course	40.09	-108.76	1655	8/1/2010	12/30/2015	2011 - 2015
ROMO	Rocky Mountain National Park	Long's Peak	40.28	-105.55	2743	4/1/1987	12/30/2015	1998 - 2015
WICA	Wind Cave National Park	Visitor Center	43.56	-103.48	1292	12/31/2003	12/30/2015	2005 - 2008; 2010 - 2014
CAMP	Wyoming Department of Environmental Quality	Campbell, WY	44.15	-105.53	1427	1/1/2005	12/31/2015	2005 - 2015
CNTL	Clean Air Status and Trends Network	Centennial, WY	41.36	-106.24	3175	5/9/1989	12/31/2015	1990 - 2015
GTHC	Clean Air Status and Trends Network	Gothic, CO	38.96	-106.99	2915	5/13/1989	12/31/2015	1990 - 2015
PNDE	Clean Air Status and Trends Network	Pinedale, WY	42.93	-109.79	2386	10/21/1988	12/31/2015	1989 - 1994; 1996 - 2015
BADL	Badlands National Park	Visitor Center	43.74	-101.94	739	10/1/1987	12/31/2014	1988 - 1991; 2004 - 2014
CRMO	Craters of the Moon National Monument & Preserve	Visitor Center	43.46	-113.56	1815	9/24/1992	12/30/2015	1993 - 2004; 2007 - 2015
GRBA	Great Basin National Park	Maintenance Yard	39.01	-114.22	2060	8/24/1993	12/30/2015	1994 - 2015
GRCA	Grand Canyon National Park	The Abyss	36.06	-112.18	2073	1/1/1993	12/30/2015	1993 - 2015
PEFO	Petrified Forest National Park	South Entrance	34.82	-109.89	1723	1/1/2002	12/30/2015	2003 - 2015
YELL	Yellowstone National Park	Water Tank	44.56	-110.40	2400	6/1/1996	12/30/2015	1997 - 2015
ZION	Zion National Park	Dalton's Wash	37.20	-113.15	1213	1/1/2004	12/30/2015	2004 - 2015

895

896 * MEEK and RANG are not located in national parks, but measurements at these two sites are also maintained by the National Park Service.

897

898

Table 2. Correlation coefficients (r) and p-value in parenthesis between the pairs of variables in winter over 2006 – 2015. Partial correlation was computed for surface temperature and seasonal 95th DM8HA by controlling the effect of PV. Boldfaced numbers indicate p-value ≤ 0.10 .

Site	Time Period	r (O ₃ vs AO)			r (AO vs temperature)	r (O ₃ vs Temperature)			Partial r
		5th	50th	95th		5th	50th	95th	95th
CANY	2006 - 2015	-0.63 (0.05)	-0.72 (0.02)	-0.73 (0.02)	0.66 (0.04)	-0.81 (<0.01)	-0.64 (0.05)	-0.64 (0.04)	-0.62 (0.06)
CAMP	2006 - 2015	0.06 (0.88)	-0.15 (0.67)	-0.30 (0.40)	0.31 (0.38)	0.11 (0.75)	-0.36 (0.31)	-0.21 (0.55)	-0.27 (0.49)
DINO	2011 - 2015	-0.29 (0.64)	-0.89 (0.04)	-0.94 (0.02)	0.90 (0.04)	-0.53 (0.36)	-0.94 (0.02)	-0.96 (0.01)	-0.95 (0.05)
MEEK	2011 - 2015	-0.88 (0.02)	-0.91 (0.01)	-0.92 (0.01)	0.93 (0.02)	-0.84 (0.07)	-0.91 (0.03)	-0.85 (0.06)	-0.96 (0.04)
RANG	2011 - 2015	-0.05 (0.93)	-0.91 (0.03)	-0.93 (0.02)	0.92 (0.03)	-0.38 (0.53)	-0.99 (<0.01)	-0.95 (0.01)	-0.92 (0.08)
MEVE	2006 - 2015	-0.53 (0.11)	-0.70 (0.02)	-0.64 (0.04)	0.53 (0.12)	-0.54 (0.10)	-0.63 (0.05)	-0.59 (0.07)	-0.28 (0.47)
ROMO	2006 - 2015	-0.09 (0.81)	-0.72 (0.01)	-0.49 (0.15)	0.50 (0.14)	-0.36 (0.31)	-0.48 (0.16)	-0.21 (0.56)	-0.14 (0.72)
WICA	2006 - 2014	0.25 (0.52)	-0.58 (0.10)	-0.39 (0.21)	0.26 (0.46)	-0.28 (0.51)	-0.50 (0.21)	-0.50 (0.20)	-0.49 (0.26)
CNTL	2006 - 2015	-0.04 (0.91)	-0.47 (0.17)	-0.38 (0.28)	-0.32 (0.37)	0.63 (0.05)	0.73 (0.02)	0.66 (0.04)	0.66 (0.05)
GTHC	2006 - 2015	-0.15 (0.67)	-0.03 (0.93)	0.04 (0.92)	0.58 (0.08)	-0.35 (0.32)	-0.23 (0.52)	-0.44 (0.20)	-0.55 (0.12)
PNDE	2006 - 2015	-0.29 (0.42)	-0.46 (0.18)	-0.05 (0.89)	0.30 (0.40)	-0.27 (0.45)	-0.09 (0.80)	-0.43 (0.21)	-0.63 (0.07)
CRMO	2008 - 2015	-0.41 (0.31)	-0.28 (0.51)	-0.10 (0.82)	0.53 (0.11)	-0.54 (0.16)	-0.72 (0.04)	-0.55 (0.16)	-0.85 (0.01)
YELL	2006 - 2015	-0.68 (0.03)	-0.77 (<0.01)	-0.46 (0.19)	0.37 (0.15)	-0.63 (0.05)	-0.43 (0.22)	-0.43 (0.22)	-0.37 (0.32)

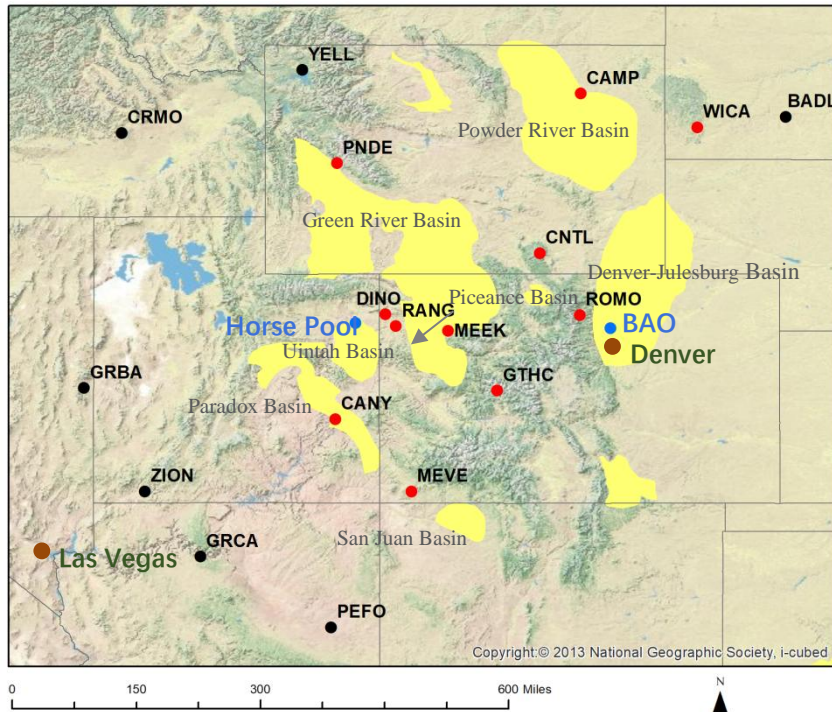


Figure 1. Topographic map of the mountain states with tight O&NG plays in the basins highlighted in yellow (<https://www.eia.gov/>). Eleven sites are located within 100km of a shale play (red dots), while seven sites are located at the periphery of the shale play (black dots). Blue dots show two campaign locations, Horse Pool and Boulder Atmospheric Observatory (BAO).

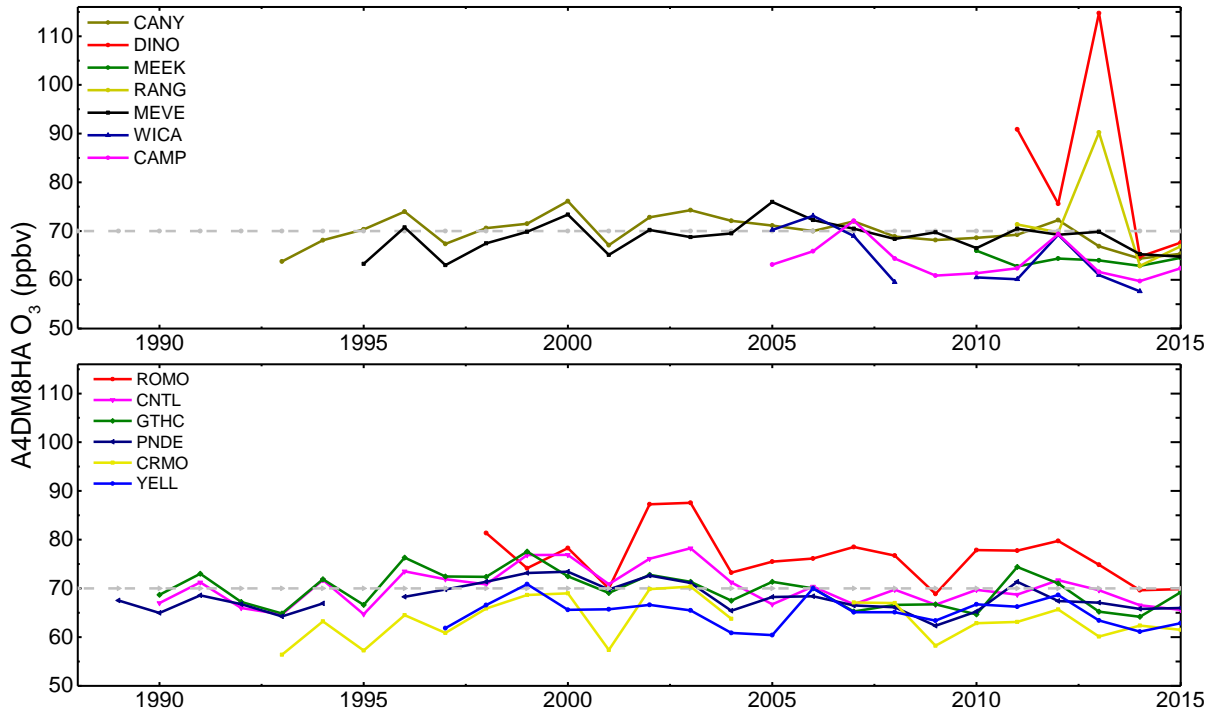


Figure 2. Time series of the A4DM8HA at each site. Dashed lines indicate the current ground-level O₃ standard (70 ppbv).

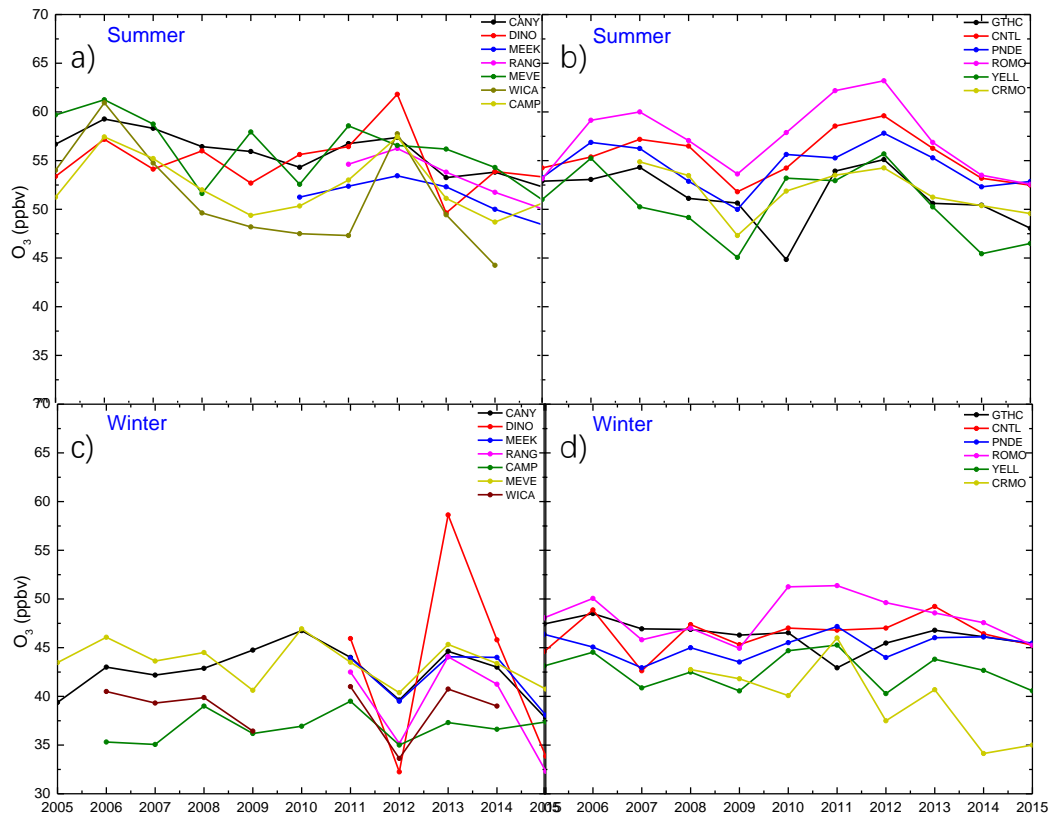


Figure 3. Time series of seasonal median values of DM8HA O₃ at each site in summer (a-b) and winter (c-d).

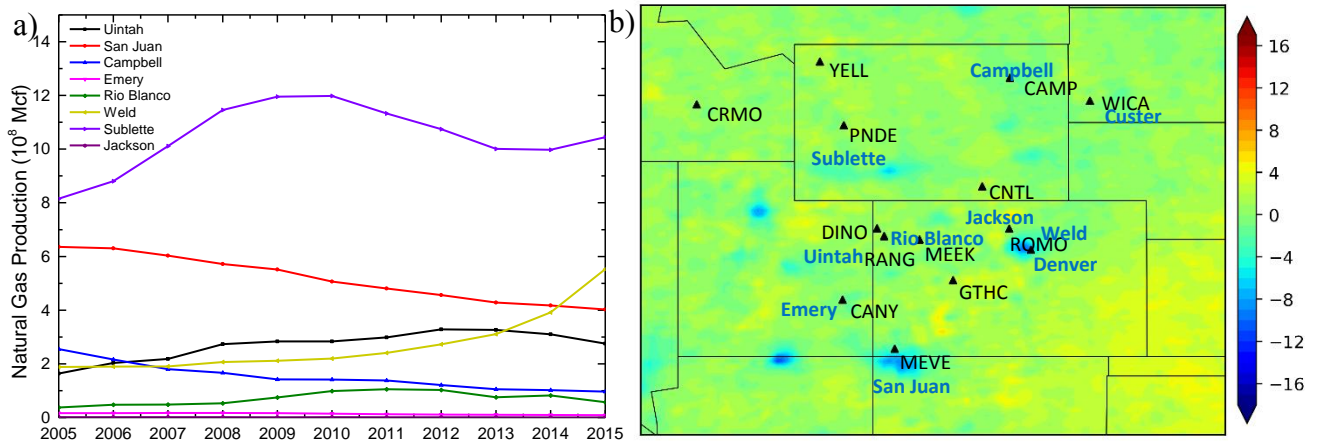


Figure 4. (a) Annual natural gas production in the counties that located in the O&NG basins over 2005 – 2015 (Data sources: the Utah Oil and Gas Program, <https://oilgas.ogm.utah.gov/oilgasweb/index.xhtml>; the Colorado Oil&Gas Conservation Commission, <http://cogcc.state.co.us/data.html>; the Wyoming Oil&Gas Conservation Commission, <http://wogcc.wyo.gov/>; the New Mexico Oil Conservation Division, <http://www.emnrd.state.nm.us/ocd/>). (b) The difference of OMI tropospheric NO₂ column densities (10¹⁴ molec.cm⁻²) in summer between periods of 2005 – 2010 and 2011 – 2015. Yellow color indicates regions where NO_x has increased between 2005 – 2010 and 2011 – 2015, while blue color indicates regions where NO_x has decreased. (Data source: Tropospheric Emission Monitoring Internet Service (TEMIS), www.temis.nl).

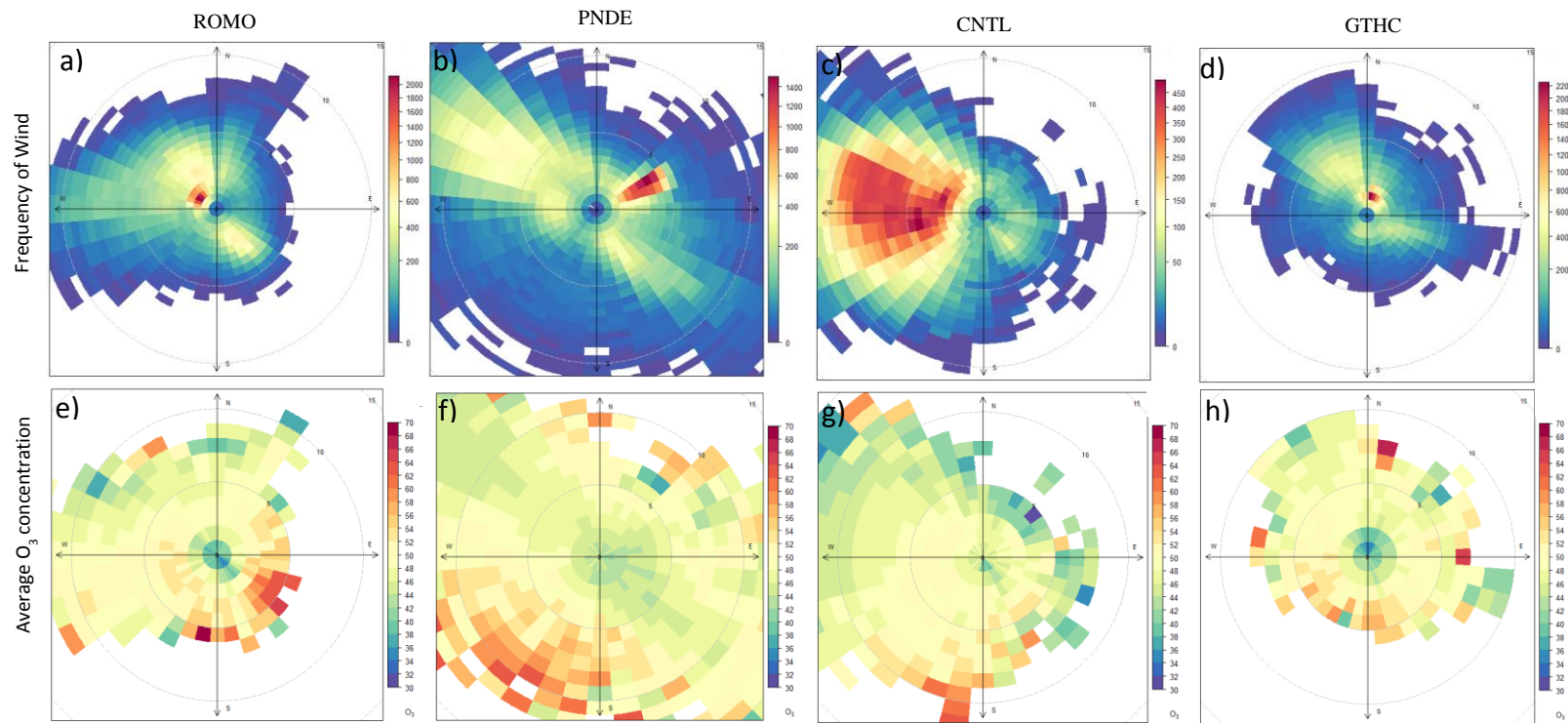


Figure 5. Frequency of wind (a-d) and average O₃ concentrations (ppbv) (e-h) binned by wind speed and wind direction at ROMO (a, e), PNDE (b, f), CNTL (c, g), and GTHC (d, h) over 2005 – 2015.

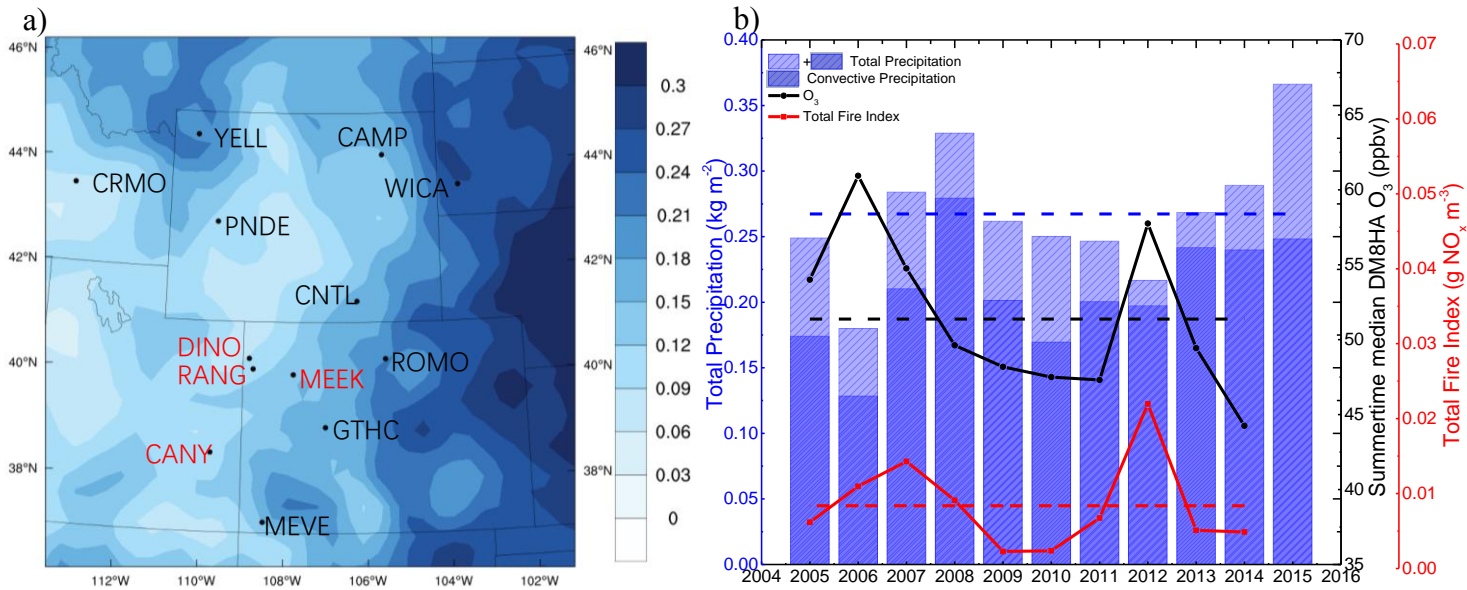


Figure 69. (a) Decadal average summertime total precipitation (kg m^{-2}) over 2005 – 2015, and the sites with low precipitation levels highlighted in red. (b) Time series of summer seasonal median DM8HA O_3 , convective precipitation, total precipitation, and total fire index at WICA.

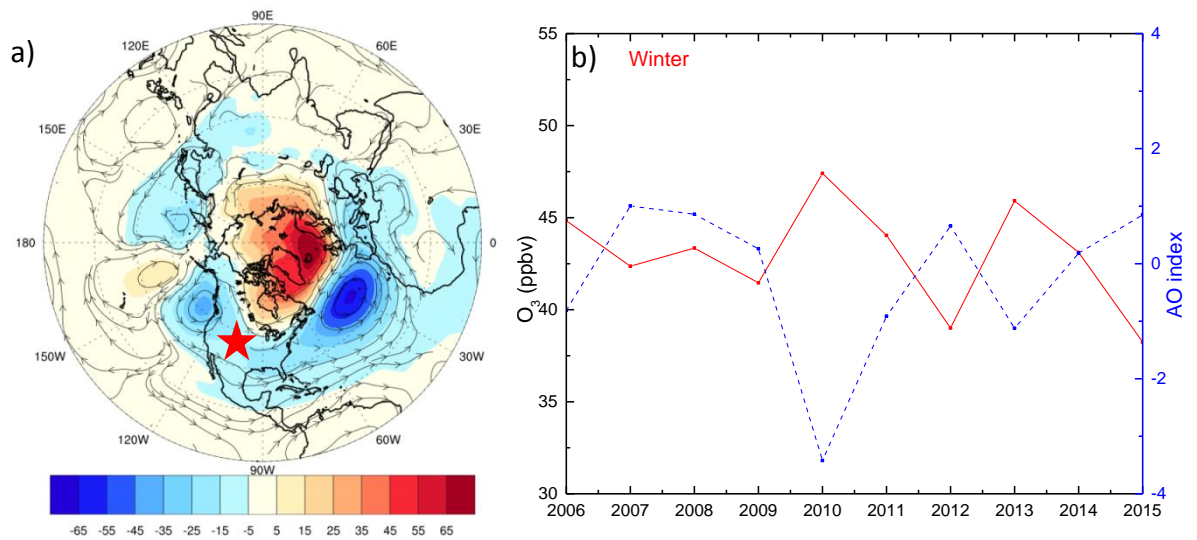


Figure 76. (a) The difference of geopotential height (m) and streamlines at 850 hPa between the high (2006, 2008, 2010, 2011, 2013) and low O₃ years (2007, 2009, 2012, 2014, 2015). (b) Time series of median DM8HA O₃ averaged over the study region and the AO index in winter. The red star indicates the study region. (Source: NCEP/NCAR reanalysis)

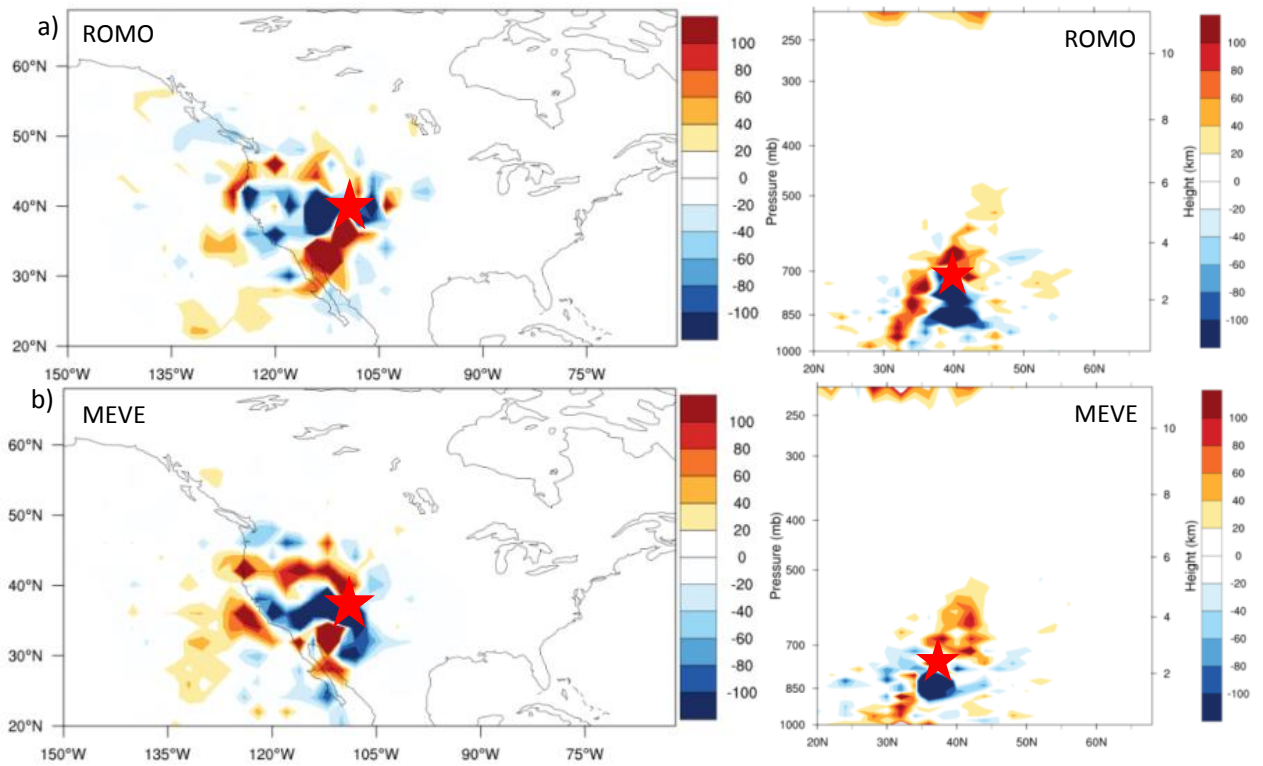


Figure 87. Maps and cross sections of differences in the number of 5-day backward trajectories originating at (a) ROMO and (b) MEVE (a) YELL, (b) MEVE, (c) WICA, (d) PNDE, (e) ROMO, and (f) CNTL between high (2006, 2008, 2010, 2011, 2013) and low O_3 years (2007, 2009, 2012, 2014, 2015). Red stars indicate study sites. The red color indicates origins of air masses reaching the study site during high O_3 years, while blue color indicates locations of major air mass sources during low O_3 years.

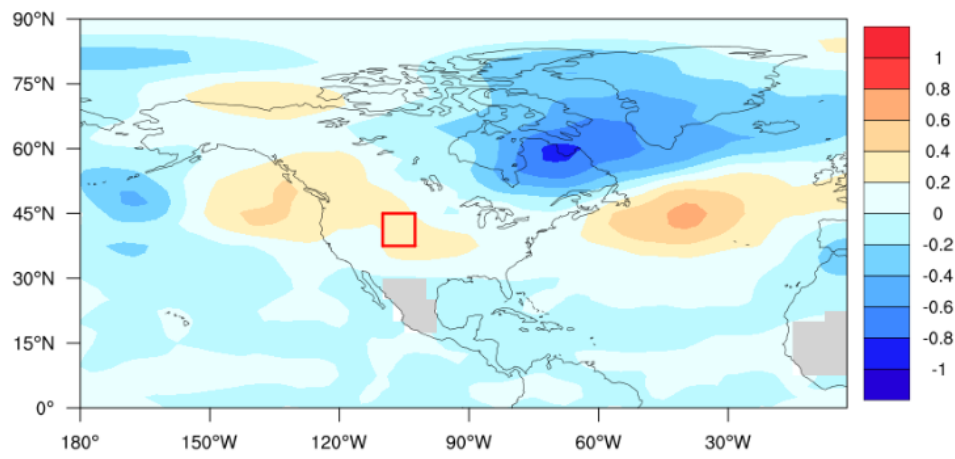


Figure 98. The difference of potential vorticity ($10^{-6} \text{ m}^2 \text{ s}^{-1} \text{ kg}^{-1} \text{ K}$) at 315 K between the high O₃ years (2006,

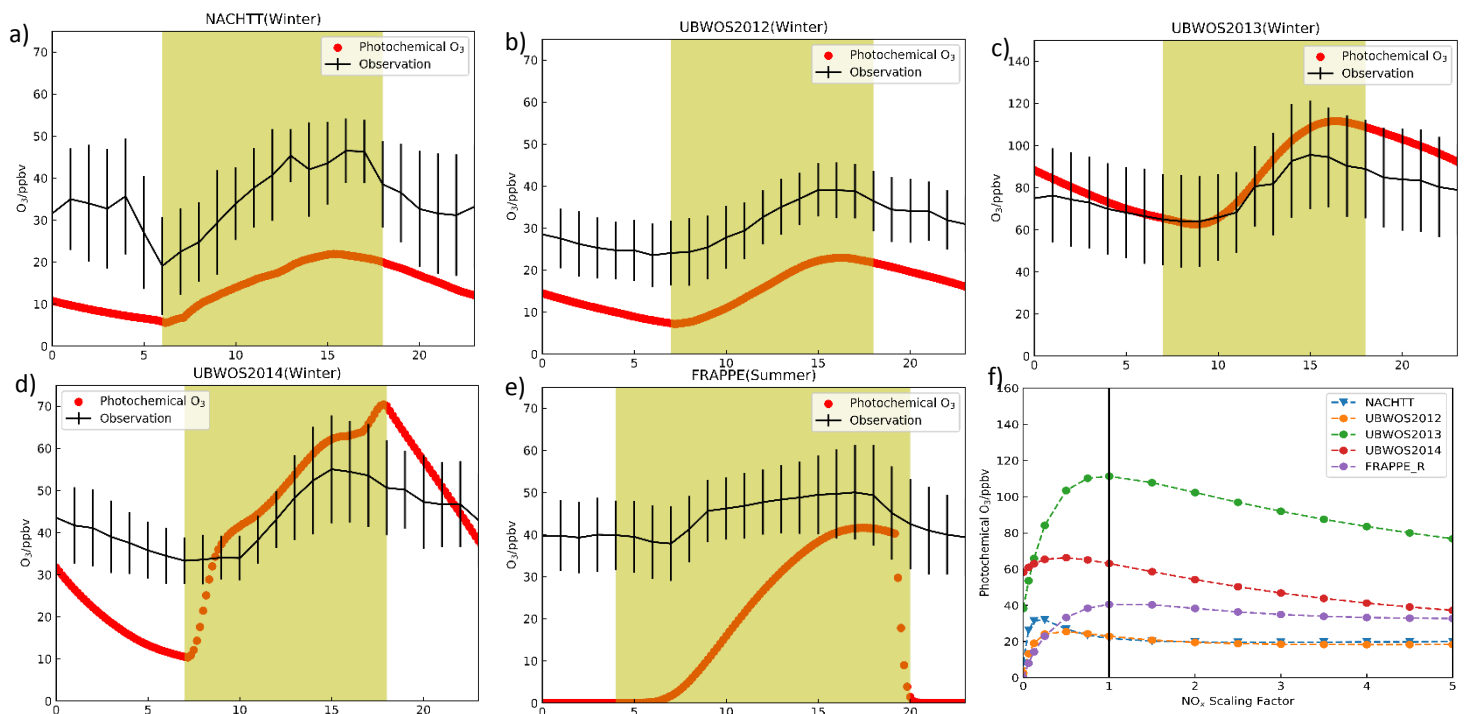


Figure 10. (a)-(e) Observed diel O₃ profile (black) and fully constrained base model calculated (red) for five campaigns. (f) NO_x sensitivity of maximum photochemical O₃ during each campaign. Shaded area indicated the time period between sunrise and sunset averaged over each campaign ~~The sensitivity of maximum photochemical O₃ to NO_x was tested by simulations with observed VOC concentrations and observed NO_x mixing ratios which was scaled by a factor from 0 to 5. NO_x scaling factor of 1 indicated observed NO_x mixing ratios.~~

Decadal Trends and Variability in Intermountain West Surface Ozone near Oil and Gas Extraction Fields

Ying Zhou¹, Huiting Mao¹, and Barkley C. Sive²

¹Department of Chemistry, State University of New York College of Environmental Science and Forestry, Syracuse, NY, 13210, USA

²National Park Service, Air Resources Division, Lakewood, CO 80225, USA

Corresponding author: H. Mao (hmao@esf.edu)

Contents of this File

Text: Section S1 to S8

Figures: S1 to ~~S3~~S4

Tables: S1 to ~~S8~~S7

S1. Locations of selected sites

~~Long term ozone (O₃) observations were available at 18 rural sites in the U.S. Intermountain West and 11 sites were located within 100 km of the shale play (Figure 1 and Table S1). Data were obtained from the National Park Service (NPS), Clean Air Status and Trends Network (CASTNET), and Wyoming Department of Environmental Quality (WDEQ).~~

S2. Identification of reference sites

~~The backward~~Backward trajectory cluster analysis was used to identify sites that were under the minimal influence of oil and natural gas (O&NG) ~~extraction~~extraction (Figure 1). ZION, GRCA, GRBA, and PEFO are located in the downwind area of Las Vegas (Figures S1c-f). Cluster analysis ~~indicated~~suggested that ~20% – 50% of air masses likely came from the direction of Las Vegas. ~~In, NE, and in~~ addition, ~30% of air masses at GRCA (Cluster 4) and PEFO (Cluster 3) passed Phoenix, AZ. Therefore, surface O₃ at ZION, GRCA, GRBA, and PEFO ~~could be~~was likely significantly influenced by ~~the nearby anthropogenic~~urban emissions. At BADL, Cluster 3 ~~indicated~~suggested that 32% of air masses was transported from the periphery of the Powder River Basin (Figure S1g). In comparison, nearly all clusters reaching YELL and CRMO were found be from the upwind areas of O&NG extraction. Therefore, YELL and CRMO were used as reference sites to investigate the decadal O₃ change.

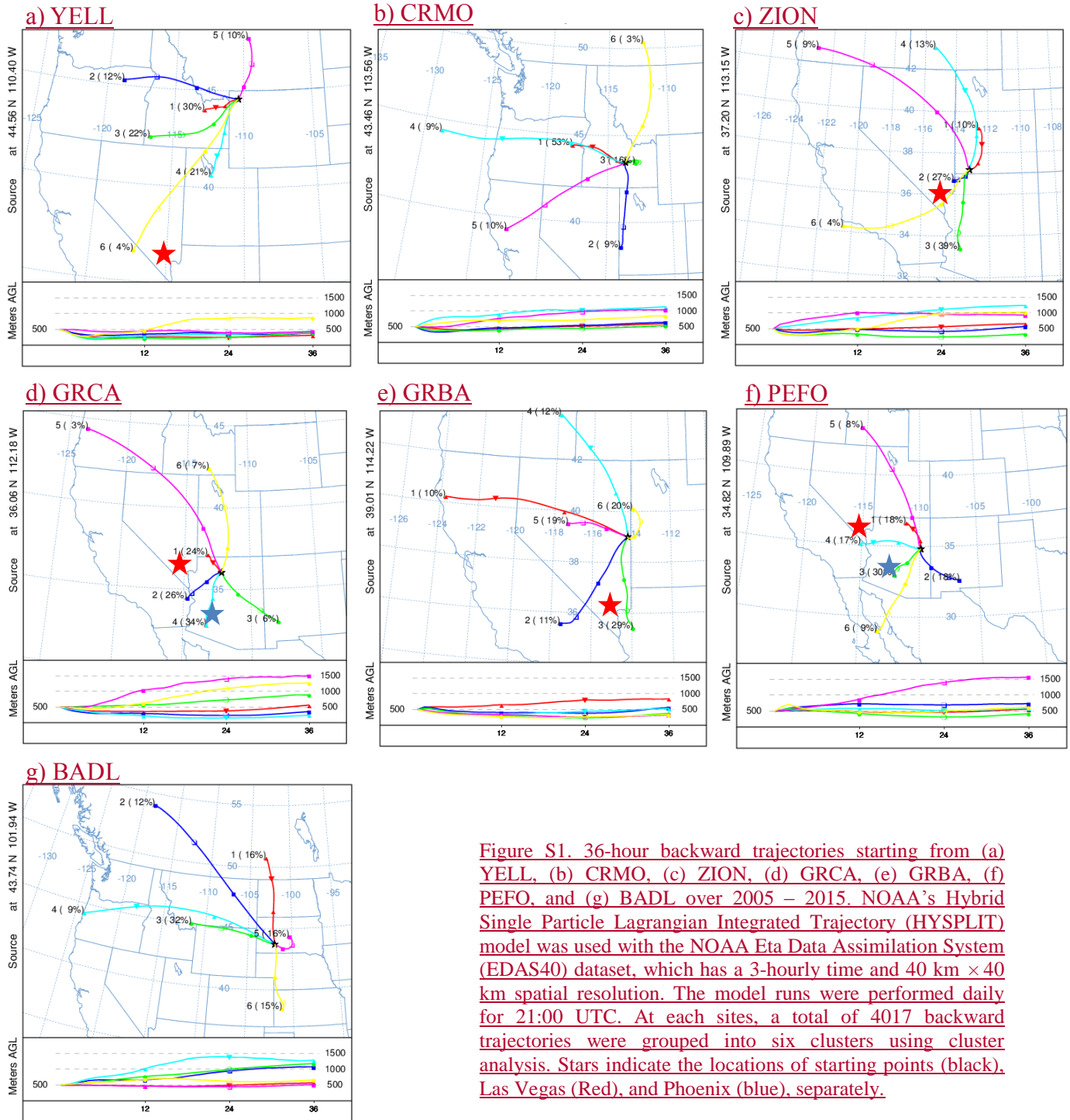


Figure S1. 36-hour backward trajectories starting from (a) YELL, (b) CRMO, (c) ZION, (d) GRCA, (e) GRBA, (f) PEFO, and (g) BADL over 2005 – 2015. NOAA’s Hybrid Single Particle Lagrangian Integrated Trajectory (HYSPLIT) model was used with the NOAA Eta Data Assimilation System (EDAS40) dataset, which has a 3-hourly time and 40 km × 40 km spatial resolution. The model runs were performed daily for 21:00 UTC. At each sites, a total of 4017 backward trajectories were grouped into six clusters using cluster analysis. Stars indicate the locations of starting points (black), Las Vegas (Red), and Phoenix (blue), separately.

Table S1. Names and locations of sites used in this study.

Site Abbreviation	Park Unit/Measurement Network	Site	Latitude	Longitude	Elevation (m)	Start Date	End Date	Year-round Measurement
CANY	Canyonlands National Park	Island in the Sky	38.46	-109.82	1809	7/1/1992	12/30/2015	1993–2015
DINO	Dinosaur National Monument	West Entrance Housing	40.29	-108.94	1463	4/1/2005	12/30/2015	2011–2015
MEEK	Meeker	Plant Science Resource Management	40.00	-107.85	1994	1/1/2010	12/30/2015	2010–2015
MEVE	Mesa Verde National Park	Area	37.20	-108.49	2165	3/1/1993	12/30/2015	1995–2015
RANG	Rangely	Golf Course	40.09	-108.76	1655	8/1/2010	12/30/2015	2011–2015
ROMO	Rocky Mountain National Park	Long's Peak	40.28	-105.55	2743	4/1/1987	12/30/2015	1998–2015
WICA	Wind Cave National Park	Visitor Center	43.56	-103.48	1292	12/31/2003	12/30/2015	2005–2008; 2010–2014
CAMP	WDEQ	Campbell, WY	44.15	-105.53	1427	1/1/2005	12/31/2015	2005–2015
CNTL	CASTNET	Centennial, WY	41.36	-106.24	3175	5/9/1989	12/31/2015	1990–2015
GTHC	CASTNET	Gothic, CO	38.96	-106.99	2915	5/13/1989	12/31/2015	1990–2015
PNDE	CASTNET	Pinedale, WY	42.93	-109.79	2386	10/21/1988	12/31/2015	1989–1994; 1996–2015
BADL	Badlands National Park	Visitor Center	43.74	-101.94	739	10/1/1987	12/31/2014	1988–1991; 2004–2014
CRMO	Craters of the Moon National Monument & Preserve	Visitor Center	43.46	-113.56	1815	9/24/1992	12/30/2015	1993–2004; 2007–2015
GRBA	Great Basin National Park	Maintenance Yard	39.01	-114.22	2060	8/24/1993	12/30/2015	1994–2015
GRCA	Grand Canyon National Park	The Abyss	36.06	-112.18	2073	1/1/1993	12/30/2015	1993–2015
PEFO	Petrified Forest National Park	South Entrance	34.82	-109.89	1723	1/1/2002	12/30/2015	2003–2015
YELL	Yellowstone National Park	Water Tank	44.56	-110.40	2400	6/1/1996	12/30/2015	1997–2015
ZION	Zion National Park	Dalton's Wash	37.20	-113.15	1213	1/1/2004	12/30/2015	2004–2015

* MEEK and RANG are not located in national parks, but measurements at these two sites are also maintained by the NPS.

S2S3. Trends in surface ozone at each site

The US EPA's ozone design value (ODV) is defined as the 3 year running mean of the annual fourth-highest daily maximum 8 hour average (DM8HA) O₃ concentration. We calculated the annual fourth highest DM8HA (A4DM8HA) for the 13 monitoring sites and their trends were examined ~~through ordinary linear least square regression~~ using Mann-Kendall before and after 2005. The trends were also calculated separately for 5th, 50th, 95th percentiles ~~of~~ DM8HA O₃ mixing ratios in summer and winter.

Table S2S1. Trends in the A4DM8HA O₃ at each site before and after 2005. Boldfaced numbers indicate p-value ≤ 0.10.

Site	Time Period	Trends	Time Period	Trends (ppbv yr ⁻¹)	Average (ppbv)
CANY	1993 - 2004	0.5561 (0.06)	2005 - 2015	-0.5458 (0.0204)	68.8
CAMP			2005 - 2015	-0.4438 (0.2524)	63.9
DINO			2011 - 2015		82.7
MEEK			2010 - 2015		64.1
RANG			2011 - 2015		72.2
MEVE	1995 - 2004	0.4553 (0.2547)	2005 - 2015	-0.7683 (<0.01)	69.4
ROMO	1998 - 2004	0.4129 (0.7899)	2005 - 2015	-0.4619 (0.2364)	75.1
WICA			2005 - 2014	-1.2116 (0.0509)	64.5
CTNL	1990 - 2004	0.65 (<68 (0.0103))	2005 - 2015	-0.0603 (0.7831)	68.4
GTHC	1990 - 2004	0.1710 (0.4662)	2005 - 2015	-0.1621 (0.6435)	68.1
PNDE	1989 - 2004	0.42 (0.33 (0.0302))	2005 - 2015	-0.0816 (0.7535)	66.8
CRMO	1993 - 2004	0.7983 (0.0602)	2007 - 2015	-0.5054 (0.2318)	63.1
YELL	1997 - 2004	-0.3018 (0.5754)	2005 - 2015	-0.1728 (0.58)	64.8

Table S3S2. Trends in seasonal 5th, 50th, and 95th ~~percentiles of percentile~~ DM8HA O₃ mixing ratios at each site in winter and summer over 2005 – 2015. Boldfaced numbers indicate p-value ≤ 0.10. Note that wintertime O₃ in a certain year referred to O₃ in January, February, and December in the previous year.

Site	Time Period	Winter			Summer			
		5th	50th	95th	Time Period	5th	50th	95th
CANY	2006 - 2015	-0.0519	-0.0733	-0.1745	2005 - 2015	-0.53	-0.5150	-0.4033
CAMP	2006 - 2015	0.1709	0.1217	-0.1716	2005 - 2015	-0.1206	-0.3228	-0.5142
DINO	-				2005 - 2015	-0.1621	-0.1115	-0.0901
MEVE	2006 - 2015	-0.4152	-0.2234	-0.4967	2005 - 2015	-0.5147	-0.6360	-0.6169
ROMO	2006 - 2015	0.2253	-0.0421	-0.2133	2005 - 2015	-0.1322	-0.1318	-0.3428
WICA	2006 - 2014	-0.2307	-0.1607	-0.3003	2005 - 2014	-0.561.60	-0.981.02	-1.3860
CTNL	2006 - 2015	0.1525	-0.13	-0.0835	2005 - 2015	-0.0306	-0.0712	0.1415
GTHC	2006 - 2015	-0.1104	-0.2423	-0.3623	2005 - 2015	-0.2518	-0.3135	-0.2325
PNDE	2006 - 2015	0.12	0.1017	-0.6927	2005 - 2015	0.2614	-0.0713	-0.1009
CRMO	2008 - 2015	-0.7176	-1.1830	-1.1012	2007 - 2015	-0.1416	-0.3454	-0.4657
YELL	2006 - 2015	-0.0604	-0.10	-0.5559	2005 - 2015	-0.2532	-0.3946	-0.1120

S4S3. Emissions in selected counties

Emissions of NOx and VOCs were obtained from EPA's National Emission ~~Inventory~~ Inventories (NEI).

Table S4S3. NO_x emissions in selected counties

County	State	Basin	NO _x emission (T _{enton})_O&NG Extraction				NO _x emission (T _{enton})_total			
			2005	2008	2011	2014	2005	2008	2011	2014
San Juan	New Mexico	San Juan Basin	263	351	14504	13906	80997	35626	44806	41902
Emery	Utah	Paradox Basin	0	0	88	158	30282	32814	22215	20729
Uintah	Utah	Uintah-Piceance Basin	0	0	10033	7412	8698	2049	11897	9407
Campbell	Wyoming	Powder River Basin	0.33	2407	505	2301	12142	22195	44429	18702
Sublette	Wyoming	Greater Green River Basin	0	5977	2501	4188	2369	9091	4970	5792
Jackson	Colorado	North Park Basin	0	0	2	107	243	442	632	573
Rio Blanco	Colorado	Uintah-Piceance Basin	7	190	1434	4021	2020	3914	5027	6997
Weld	Colorado	Denver-Julesburg Basin	0	76	12478	17892	13112	20088	32696	33275
Custer	South Dakota		0	0	2.25	0.45	1156	1309	1727	1373

Table S5S4. VOC emissions in selected counties

County	State	Basin	VOC emission (T _{enton})_O&NG Extraction				VOC emission (T _{enton})_total			
			2005	2008	2011	2014	2005	2008	2011	2014
San Juan	New Mexico	San Juan Basin	142	512	22089	32819	8858	58095	88840	97096
Emery	Utah	Paradox Basin	0	0	459	549	1715	43441	46945	37107
Uintah	Utah	Uintah-Piceance Basin	0	0	76502	86915	4545	40044	116207	126578
Campbell	Wyoming	Powder River Basin	52	2697	6703	8559	9558	35514	48870	34363
Sublette	Wyoming	Greater Green River Basin	5	15863	9079	58304	1558	70276	45282	86146
Jackson	Colorado	North Park Basin	28	57	516	688	1125	17402	20813	12850
Rio Blanco	Colorado	Uintah-Piceance Basin	0.4	1092	23432	6141	1647	34518	57809	38601
Weld	Colorado	Denver-Julesburg Basin	0	713	104473	91709	12846	52991	150982	116146
Custer	South Dakota		0	0	12	1	1789	27132	29169	19210

S5. Wintertime O₃ at Edmonton, Alberta, Canada

Ozonesonde data at Edmonton were obtained from the World Ozone and Ultraviolet Radiation Data Center (<http://woude.org/data/products/ozonesonde/>). Significant negative correlation ($r = -0.49$, $p = 0.01$) was found between lower tropospheric O₃ at Edmonton and the AO index over the winter of 1988–2014 (Figure S2).

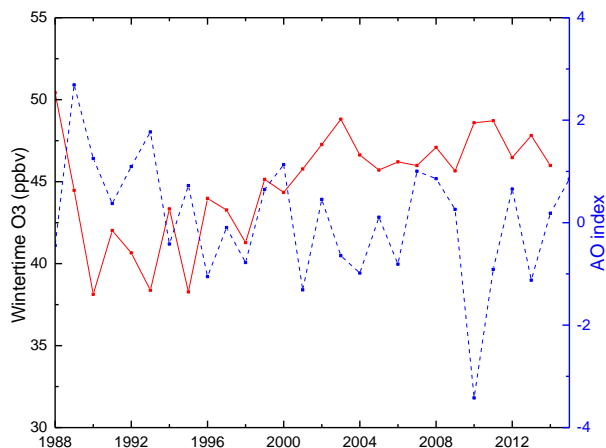


Figure S2. Time series of lower tropospheric (2–5 km) O₃ at Edmonton (53.55°N, 114.10°W) and the AO index in winter.

S6S4. Fire index

The NOAA's Lagrangian dispersion model, Hybrid Single-Particle Lagrangian Integrated Trajectory (HYSPLIT) model, was used to estimate O₃ concentrations determined by wildfire emissions. HYSPLIT simulated the long-range and mesoscale transport, diffusion, and dry and wet deposition of gas or particles (Draxler & Hess, 1998). The National Center for Environmental Prediction (NCEP) Eta Data Assimilation System (EDAS40) datasets, with a 3-hourly time and 40 km × 40 km spatial resolution, were used to drive the Lagrangian dispersion model. For each day over summer 2005–2015, 250,000 particles were released at a constant hourly rate during the first 24 h at a height of 100 m ~~over~~at each measurement site. A decay half-life of five days occurred to the particle mass (Lu et al., 2016) and the particles were traced

backward for five days. The retroplumes of each sample were calculated daily in $0.25^\circ \times 0.25^\circ$ horizontal resolution from the surface to 5 km. In total, we have computed over 4950 HYSPLIT retroplumes for each Intermountain West site.

The Global Fire Emissions Database version 4.1 (GFED4s) ~~were~~was used to provide information ~~of~~on biomass burning emissions. GFED4s ~~had~~has a spatial resolution of $0.25^\circ \times 0.25^\circ$ and ~~contained~~contains monthly burned area, fire carbon and dry matter emissions (DM), as well as daily fraction and contributions of different fire types to the total emissions since 2003. The fire types ~~included~~include savanna, grassland, and shrubland fires, boreal forest fires, temperate forest fires, tropical deforestation and degradation fires, peatland fires, and agricultural waste burning. Biomass burning ~~was complex and the~~ emissions ~~depended~~depend greatly on the ecosystem type (Jaffe et al., 2008). Akagi et al. (2011) found that wildfire emissions had a relatively high VOC/NO_x ratio of ~10 – 100 and O₃ production in smoke plumes was very sensitive to NO_x concentrations. Different from previous studies (Jaffe et al., 2008; Lu et al., 2016) using monthly or daily wildfire burned areas, we estimated daily wildfire NO_x emissions using monthly DM emissions, daily fraction, and fractional contribution of fire types in combination of emission factors (Akagi et al. 2011). Based on Lu et al. (2016), we then calculated a fire index (FI) as the product of daily HYSPLIT residence time and daily wildfire NO_x emission, in units of g NO_x m⁻³. The sum of FI over the 5-day period was defined as total fire index (TFI):

$$FI(n) = \sum_i \sum_j \sum_k E_{DM}(i, j) \times t_r(i, j, n) \times F_{daily}(i, j, n) \times F_{type}(k)$$

$$TFI = \sum_{n=1}^5 FI(n)$$

where $E_{DM}(i, j)$ was the monthly wildfire dry matter emission in the model grid cell i (longitude) and j (latitude), $F_{daily}(i, j, n)$ was the daily fraction of wildfire emissions, $F_{type}(k)$ was the NO_x

emission factor from fire type k , $t_{r(i, j, n)}$ was HYSPLIT calculated daily residence time, and n defined the backward day in the 5-day period. The summertime wildfire NO_x impacts were computed by averaging the daily TFI index.

S7S5. Impacts of wildfire emissions on summertime O_3

In contrast to wintertime O_3 levels, summertime median DM8HA O_3 displayed significant interannual variations with large differences between sites (Figure 3). The TFI, calculated with HYSPLIT dispersion model simulations and wildfire NO_x emissions, varied showed large interannual variation at each site over 2005 – 2015 (Figure S3S2). In 2012, the western U.S. experienced widespread drought with hot weather causing frequent wildfires across the region (Abeleira & Farmer, 2017). The decadal highest TFI value (0.013 – 0.052 $\text{g NO}_x \text{ m}^{-3}$) in summer 2012 were observed at CRMO and YELL, as well as 9 other sites (DINO, MEEK, RANG, ROMO, WICA, CAMP, CNTL, PNDE, and GTHC) (Figure S3S2), which was mostly consistent with the observed decadal highest summertime median DM8HA O_3 at the same sites except WICA (54 – 65 ppbv).

Significant positive correlations between summertime O_3 and TFI were found at the reference site YELL, as well as at CANY, CAMP, DINO, MEVE, WICA, CNTL, GTHC, and PNDE during their respective time periods over 2005 – 2015 (Table 2S5). It should be noted that significant correlation was correlations were found for seasonal 75th or 95th percentiles percentile DM8HA O_3 mixing ratios with TFI at YELL, CANY, GTHC, PNDE, and MEVE. Strong correlations, albeit not statistically significant, were also found between TFI and summertime 95th percentile DM8HA O_3 at RANG (Table S6S5). As indicated by data at the reference site YELL, the wildfire emissions had a larger impact on high O_3 levels in summer over the Intermountain West. While wintertime O_3 at CANY, DINO, and RANG was strongly impacted

by photochemical production from O&NG emissions within the basins (Section 56), during the summer, the interannual variability of O₃ at 8 out of 11 sites near the O&NG extraction fields appeared to be predominantly impacted by photochemical production from wildfire emissions.

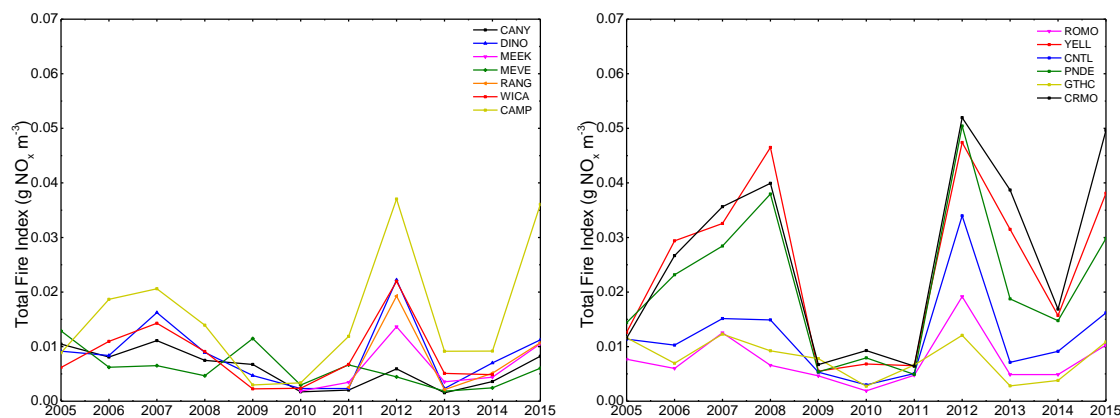


Figure S3S2. Time series of summertime total fire index at each site.

Table S6S5. Correlation coefficients (r) and p-values in parenthesis between the pairs of variables over the summer of 2005 – 2015. Boldfaced numbers indicate p-value ≤ 0.10.

Site	Time Period	r(O ₃ vs TFI)			Partial r 95th	Regression Intercept_50th	r(O ₃ vs Relative Humidity)			Partial r 5th
		5th	50th	95th			5th	50th	95th	
CANY	2005 - 2015	0.20 (0.55)	0.47 (0.14)	0.37 (0.26)	0.32 (0.40)	54.01	-0.65 (0.08)	-0.50 (0.11)	-0.01 (0.97)	-0.61 (0.07)
CAMP	2005 - 2015	0.33 (0.33)	0.57 (0.06)	0.50 (0.12)	0.22 (0.57)	50.08	-0.45 (0.19)	-0.92 (<0.01)	-0.66 (0.04)	-0.88 (<0.01)
DINO	2005 - 2015	0.62 (0.04)	0.58 (0.06)	0.62 (0.04)	0.67 (0.10)	52.42	-0.14 (0.72)	-0.18 (0.64)	-0.21 (0.59)	0.74 (0.06)
MEEK	2010 - 2015	0.13 (0.81)	0.01 (0.99)	0.45 (0.37)	0.35 (0.56)	51.28	-0.77 (0.06)	-0.71 (0.11)	-0.31 (0.55)	-0.85 (0.07)
RANG	2011 - 2015	0.34 (0.57)	0.26 (0.67)	0.76 (0.24)	0.07 (0.92)	52.58	-0.90 (0.03)	-0.62 (0.26)	-0.32 (0.60)	-0.91 (0.09)
MEVE	2005 - 2015	0.39 (0.24)	0.50 (0.11)	0.66 (0.03)	0.42 (0.26)	53.21	-0.49 (0.12)	-0.46 (0.14)	-0.36 (0.28)	-0.43(0.25)
ROMO	2005 - 2015	0.28 (0.39)	0.40 (0.22)	0.40 (0.21)	0.53 (0.12)	54.89	-0.40 (0.22)	-0.67 (0.02)	-0.80 (<0.01)	-0.58 (0.09)
WICA	2005 - 2014	0.65 (0.04)	0.71 (0.02)	0.57 (0.08)	-0.42 (0.30)	46.18	-0.71 (0.02)	-0.97 (<0.01)	-0.90 (<0.01)	-0.79 (0.02)
CNTL	2005 - 2015	0.59 (0.06)	0.49 (0.12)	0.36 (0.28)	-0.13 (0.83)	53.69	-0.69 (0.13)	-0.74 (0.09)	-0.38 (0.45)	-0.44 (0.46)
GTHC	2005 - 2015	0.28 (0.40)	0.55 (0.08)	0.49 (0.03)	0.67 (0.09)	47.76	0.24 (0.65)	-0.19 (0.72)	-0.21 (0.69)	0.45 (0.45)
PNDE	2005 - 2015	0.46 (0.16)	0.41 (0.21)	0.53 (0.09)	-0.06 (0.89)	52.96	-0.58 (0.10)	-0.67 (0.55)	-0.78 (0.01)	-0.70 (0.05)
CRMO	2007 - 2015	-0.45 (0.22)	0.33 (0.38)	0.29 (0.44)	-0.26 (0.58)	50.58	0.36 (0.48)	-0.89 (0.02)	-0.91 (0.01)	-0.87 (0.05)
YELL	2005 - 2014	0.01 (0.49)	0.14 (0.34)	0.50 (0.05)	-0.03 (0.95)	49.57	-0.56 (0.04)	-0.70 (0.01)	-0.81 (<0.01)	-0.70 (0.03)

Regression equations were used to quantify the relationship between seasonal median DM8HA O₃ and TFI, where the intercepts from the equations represented decadal summertime median DM8HA O₃ values in the absence of fires (Jaffe et al., 2008). No significant positive correlation was found between summertime O₃ and TFI at ROMO, and TFI, while the O₃

concentration without wildfires (55 ppbv), based on the intercept value, was found to be the highest at this site. As stated in Section 4, ROMO was influenced by the high O₃ concentrations from the southeast over 2005 – 2015 (Figure 5). Summertime O₃ at ROMO was under strong influence of frequent transport of highly polluted air masses **emerging** from the greater Denver area, which likely dominated over the impact of wildfire emissions during the decade of the study period. Reddy and Pfister (2016) also found significant correlations between July DM8HA O₃ and 500hPa heights, particularly in areas of elevated terrain near urban sources of O₃ precursors.

S6. Wintertime O₃ at Edmonton, Alberta, Canada

Ozonesonde data at Edmonton were obtained from the World Ozone and Ultraviolet Radiation Data Center (<http://woudc.org/data/products/ozonesonde/>). Significant negative correlation ($r = -0.49$, $p = 0.01$) was found between lower tropospheric O₃ at Edmonton and the AO index over the winter of 1988 – 2014 (Figure S3).

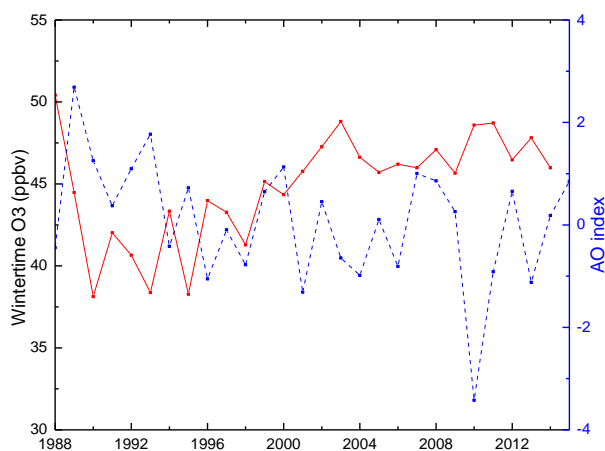


Figure S3. Time series of lower tropospheric (2 – 5 km) O₃ at Edmonton (53.55 °N, 114.10 °W) and the AO index in winter.

S7. Contributions of transport from the Arctic and West Coast

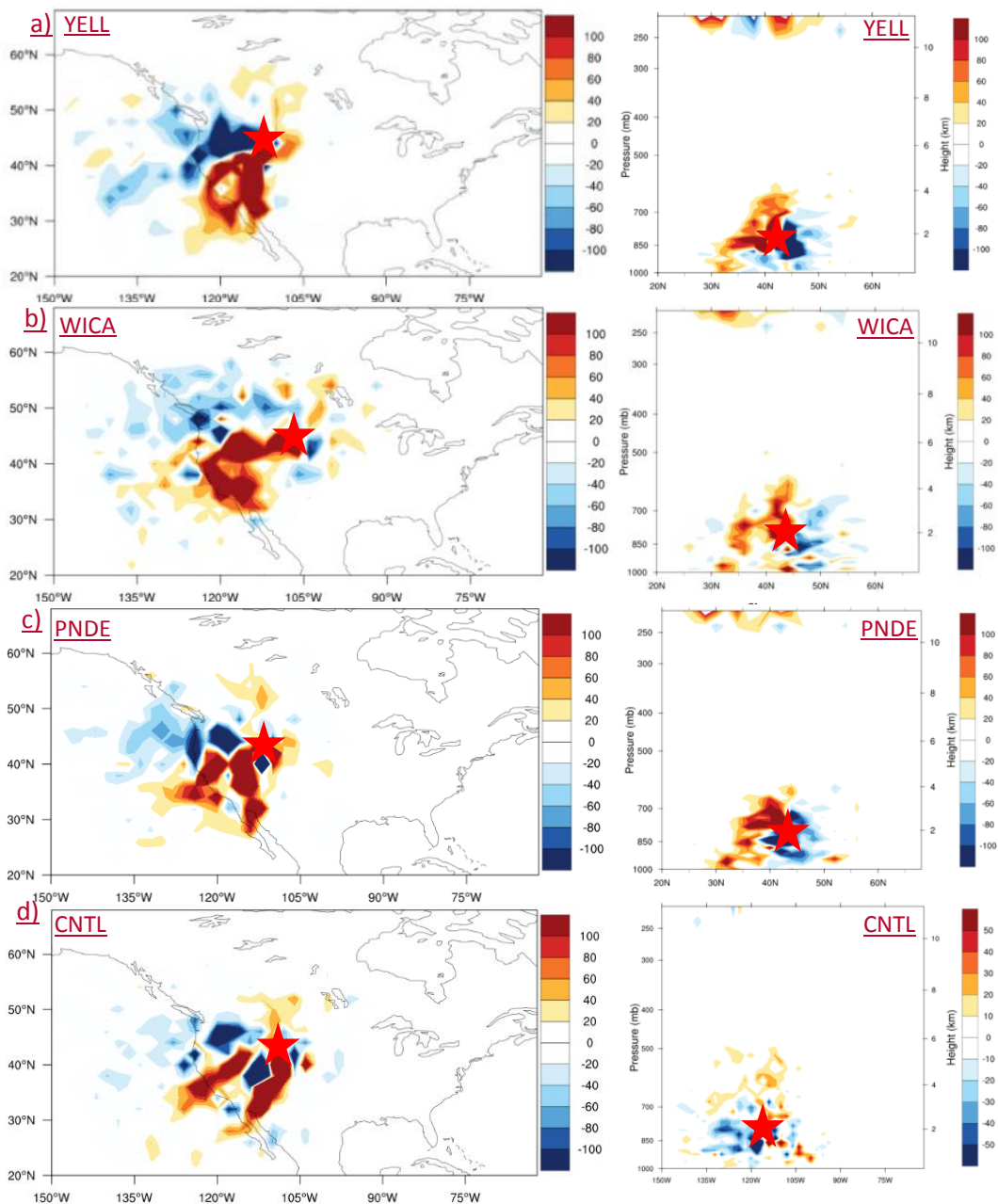


Figure S4. Maps and cross sections of differences in the number of 5-day backward trajectories originating at (a) YELL, (b) WICA, (c) PNDE, (d) CNTL, and between high (2006, 2008, 2010, 2011, 2013) and low O_3 years (2007, 2009, 2012, 2014, 2015). Red stars indicate study sites. Red color indicates regions and heights from where more air masses reached the study site in high O_3 years, while blue color indicates locations of air mass sources in low O_3 years.

S8. BOXMOX Model Simulations

S8.1 Field Campaigns

Surface observations were obtained from five field campaigns to constrain model simulations (Tables ~~S7-8S6-7~~). The Nitrogen, Aerosol Composition, and Halogens on a Tall Tower (NACHTT) campaign was conducted at the National Oceanic and Atmospheric Administration’s Boulder Atmospheric Observatory (BAO). BAO is located in a primarily agricultural region and is very close to major urban areas. It is ~35 km north of Denver and ~30 km east of Boulder. In addition, the site is located within the Denver-Julesburg Basin, which is an active ~~oil and gas~~O&NG exploration and production region. The Uintah Basin Winter Ozone Studies (UBWOS) were a set of field campaigns held at Horse Pool during January and February of 2012, 2013, and 2014. Horse Pool is a remote site, located within the oil and gas basin of northeastern Utah. In summer 2014, the NSF Front Range Air Pollution and Photochemistry Experiment (FRAPPÉ) and the NASA Deriving Information on Surface Conditions from Column and Vertically Resolved Observations Relevant to Air Quality (DISCOVER-AQ) field campaigns conducted aircraft, mobile, and ground-based measurements over 15 locations across the Front Range. In this study, we used field measurements at ROMO-LP. All campaign data were available at <https://esrl.noaa.gov/csd/groups/csd7/measurements/>.

Table ~~S7. Name~~S6. Names and locations of campaign sites used in this study

Campaign	Time Period	State	Site	Elevation/km	Latitude	Longitude
NACHTT	02182011-03132011	Colorado	BAO	1.58	40.05	-105.01
UBWOS2012	01172012-02222012	Utah	Horse Pool	1.53	40.14	-109.47
UBWOS2013	02012013-02212013	Utah	Horse Pool	1.53	40.14	-109.47
UBWOS2014	01182014-02142014	Utah	Horse Pool	1.53	40.14	-109.47
FRAPPÉ	07172014-09032014	Colorado	ROMO-LP	2.74	40.28	-105.55

S8.2 Photolysis Rates

The model used the NCAR TUV radiation model to calculate photolysis frequencies, with inputs for latitude, longitude, altitude, Julian day, temperature, surface pressure, total O₃ column, and albedo. Inputs of surface temperature and pressure were constrained to measurements from field campaigns, while total O₃ column was derived from averaged OMI data. The TUV calculated photolysis frequencies were then scaled to the observed $j(\text{NO}_2)$, except for $j(\text{O}^1\text{D})$. Measurement of $j(\text{NO}_2)$ was not available for UBWOS2013, UBWOS2014, and FRAPPÉ. Instead, total downwelling radiation measurements from these three campaigns were used to calculate photolysis frequencies by comparison with data from UBWOS2012 (Edwards et al. 2014). Polynomial regression was used to find the relationship between downwelling solar radiation versus $j(\text{NO}_2)$ using data from UBWOS2012 (E1). Then, $j(\text{NO}_2)$ during UBWOS2013, UBWOS2014, and FRAPPÉ was calculated using the derived equation (E1).

$$j(\text{NO}_2) = 5.509 \times 10^{-6} + 1.425 \times 10^{-5} \times \text{Radiation}_{\text{downwelling}} - 4.760 \times 10^{-9} \times \text{Radiation}_{\text{downwelling}}^2 \quad \text{--- E1}$$

$$\underline{j(\text{NO}_2) = 1.425 \times 10^5 \text{ Radiation}_{\text{downwelling}} + 4.760 \times 10^9 \text{ Radiation}_{\text{downwelling}}^2 \quad \text{(E1)}}$$

S8.3 Turbulent Mixing

Mixing ratios of CO, CH₄, NO, NO₂, and non-methane VOCs were constrained to observations by introducing turbulent mixing. This was represented by adding the background concentration of a species outside the box (Knote et al., 2015).

$$\frac{\partial c_{\text{box}}}{\partial t} = \frac{1}{\tau} (c_{\text{bg}} - c_{\text{box}}(t = t_0))$$

$$c_{\text{box}}(t = t_0 + \Delta t) = c_{\text{box}}(t = t_0) + \frac{\partial c_{\text{box}}}{\partial t} \cdot \Delta t$$

Where t_0 was the beginning of the time step, τ the mixing time-scale, c_{bg} the background concentrations of a species i outside the box, and c_{box} the initial concentration of the species i .

S8.4 Physical loss

First order rate constants were used to simulate all non-chemical loss in the model due to surface deposition. ~~Dry~~A dry deposition ~~rates~~velocity of 0.4 cm/s ~~were~~was used for O_3 over the continent and 0.07 cm/s over the snow, based on Hauglustaine et al. (1994).

~~TableS8~~TableS7. Chemical observations used to inform the box model analysis in this analysis.

Compound	Observational technique				
	NACHTT	UBWOS2012	UBWOS2013	UBWOS2014	FRAPPÉ
O_3	CRDS	CRDS	CRDS	CRDS	
H_2O					
NO	CRDS	CRDS	CRDS	CRDS	No_noxbox
NO_2	CRDS	CRDS	CRDS	CRDS	NO2_Noxbox
N_2O_5	CRDS	CRDS	CRDS	CRDS	
HNO_3	CIMS	CIMS	CIMS	HR-TOF-CIMS	
HONO	CIMS	CIMS	CIMS	HR-TOF-CIMS	
CO	Thermo 48C	VUF	VUF	VUF	
Alkanes					
Methane	1.8 ppmv	CRDS	CRDS	CRDS	1.8 ppmv
Ethane	GC-MS*	GC-MS	GC-FID	GC-MS	GC-MS*
Propane	GC-MS*	GC-MS	GC-FID	GC-MS	GC-MS*
n-Butane	GC-MS*	GC-MS	GC-FID	GC-MS	GC-MS*
iso-Butane	GC-MS*	GC-MS	GC-FID	GC-MS	GC-MS*
n-Pentane	GC-MS*	GC-MS	GC-FID	GC-MS	GC-MS*
iso-Pentane	GC-MS*	GC-MS	GC-FID	GC-MS	GC-MS*
n-Hexane	GC-MS*	GC-MS	GC-FID	GC-MS	GC-MS*
n-Heptane	GC-MS*	GC-MS	GC-FID	GC-MS	GC-MS*
n-Octane	GC-MS*	GC-MS		GC-MS	GC-MS*
n-Nonane	GC-MS*	GC-MS		GC-MS	GC-MS*
n-Decane	GC-MS*	GC-MS		GC-MS	
Undecane	GC-MS	GC-MS			
2-Methylpentane	GC-MS*	GC-MS	GC-FID	GC-MS	
3-Methylpentane	GC-MS*	GC-MS	GC-FID	GC-MS	
2,2-Dimethylbutane	GC-MS*	GC-MS	GC-FID	GC-MS	
2,3-Dimethylbutane	GC-MS*				
2-Methylhexane	GC-MS*				

3-Methylhexane				GC-MS	
Cyclohexane	GC-MS*	GC-MS	PTR-MS ¹	GC-MS	
Neopentane	GC-MS*	GC-MS	GC-FID		
Aromatics					
Benzene	GC-MS*	GC-MS	GC-FID	GC-MS	GC-MS*
Toluene	GC-MS*	GC-MS	PTR-MS	GC-MS	GC-MS*
Ethyl Benzene	GC-MS*	GC-MS	PTR-MS ¹	GC-MS	GC-MS*
n-Propyl Benzene	GC-MS*	GC-MS	PTR-MS ¹	GC-MS	
iso-Propyl Benzene	GC-MS*	GC-MS	PTR-MS ¹	GC-MS	
m-Xylene	GC-MS*	GC-MS	PTR-MS ¹	GC-MS	GC-MS*
p-Xylene	GC-MS*	GC-MS		GC-MS	GC-MS*
o-Xylene	GC-MS*	GC-MS	PTR-MS ¹	GC-MS	GC-MS*
1,3,5-Trimethylbenzene	GC-MS*	GC-MS	PTR-MS ¹	GC-MS	
1,2,3-Trimethylbenzene	GC-MS*	GC-MS	PTR-MS ¹	GC-MS	
1,2,4-Trimethylbenzene	GC-MS*	GC-MS	PTR-MS ¹	GC-MS	
m-Ethyltoluene	GC-MS*			GC-MS	
p-Ethyltoluene	GC-MS*			GC-MS	
o-Ethyltoluene	GC-MS*	GC-MS	PTR-MS ¹	GC-MS	
Styrene	GC-MS*	GC-MS			
Alkenes and Alkynes					
Ethyne (Acetylene)	GC-MS*	GC-MS	GC-FID	GC-MS	GC-MS*
Ethene	GC-MS*	GC-MS	GC-FID	GC-MS	GC-MS*
Propene	GC-MS*	GC-MS	GC-FID	GC-MS	GC-MS*
1-Butene	GC-MS*				GC-MS*
trans-2-Butene	GC-MS*				GC-MS*
cis-2-Butene	GC-MS*				GC-MS*
iso-Butene					GC-MS*
1-Pentene	GC-MS*				
trans-2-Pentene	GC-MS*				
cis-2-Pentene	GC-MS*				
2-Methyl-1-Butene	GC-MS*				
2-Methyl-2-Butene	GC-MS*				
1,3-Butadiene		GC-MS			
Aldehydes and Ketones					
Acetone	GC-MS	GC-MS	PTR-TOF-MS	GC-MS	PTR-MS
2-Butanone (Methyl Ethyl Ketone)	GC-MS	GC-MS	PTR-TOF-MS	GC-MS	PTR-MS
Formaldehyde	PTR-MS	PTR-MS	PTR-MS	PTR-TOF-MS	
Acetaldehyde	GC-MS	GC-MS	PTR-TOF-MS	GC-MS	PTR-MS
Propanal	GC-MS	GC-MS		GC-MS	
Butanal		GC-MS		GC-MS	

Hexanal		GC-MS		GC-MS	
2-Propenal (Acrolein)					
Benzaldehyde		GC-MS			
Alcohols					
Methanol	GC-MS	GC-MS	PTR-TOF-MS	GC-MS	PTR-MS
Ethanol	GC-MS	GC-MS			
iso-Propanol	GC-MS				
1-Butanol	GC-MS				
Biogenics					
Isoprene	GC-MS	GC-MS			GC-MS*
Methyl Vinyl Ketone	GC-MS	GC-MS	PTR-TOF-MS	PTR-TOF-MS	PTR-MS
Methacrolein	GC-MS	GC-MS			PTR-MS
α -Pinene	GC-MS*		PTR-TOF-MS		GC-MS*
β -Pinene	GC-MS*		PTR-TOF-MS		GC-MS*
Limonene	GC-MS*				
Alkyl Nitrates					
Methyl Nitrate	GC-MS*	GC-MS			GC-MS*
Ethyl Nitrate	GC-MS*	GC-MS		GC-MS	GC-MS*
n-Propyl Nitrate	GC-MS*	GC-MS		GC-MS	GC-MS*
iso-Propyl Nitrate	GC-MS*	GC-MS		GC-MS	GC-MS*
n-Butyl Nitrate				GC-MS	
2-Butyl Nitrate	GC-MS*				GC-MS*

*indicated that VOCs were collected with canister first and then measured with GC-MS.

[List of Acronyms in Table S7](#)

[CRDS – Cavity Ring Down Spectroscopy](#)

[GC-FID – Gas Chromatograph Flame Ionization Detector](#)

[GC-MS – Gas Chromatograph Mass Spectrometry](#)

[HR-TOF-MS – High Resolution Time-of-Flight Mass Spectrometry](#)

[PTR-MS – Proton Transfer Reaction Mass Spectrometry](#)

[PTR-TOF-MS – Proton Transfer Reaction Time-of-Flight Mass Spectrometry](#)

References

Edwards, P.M., Brown, S.S., Roberts, J.M., Ahmadov, R., Banta, R.M., DeGouw, J. A., Dubé W.P., Field, R. A., Flynn, J.H., Gilman, J.B., Graus, M., Helmig, D., Koss, A., Langford, A.O., Lefer, B.L., Lerner, B.M., Li, R., Li, S.-M., McKeen, S. A., Murphy, S.M., Parrish, D.D., Senff, C.J., Soltis, J., Stutz, J., Sweeney, C., Thompson, C.R., Trainer, M.K., Tsai, C., Veres, P.R., Washenfelder, R. a., Warneke, C., Wild, R.J., Young, C.J., Yuan, B., Zamora, R: High winter ozone pollution from carbonyl photolysis in an oil and gas basin. *Nature*, 514, 351-354, <https://doi.org/10.1038/nature13767>, 2014.

Hauglustaine, D.A., Granier, C., Brasseur, G.P., and M égie, G.: The importance of atmospheric chemistry in the calculation of radiative forcing on the climate system. *Journal of Geophysical Research*, 99, doi:10.1029/93JD02987.issn:0148-0227, 1994.

Knote, C., Tuccella, P., Curci, G., Emmons, L., Orlando, J.J., Madronich, S., Bar ó R., Jim énez-Guerrero, P., Luecken, D., Hogrefe, C., Forkel, R., Werhahn, J., Hirtl, M., Pérez, J.L., San José R., Giordano, L., Brunner, D., Yahya, K., Zhang, Y.: Influence of the choice of gas-phase mechanism on predictions of key gaseous pollutants during the AQMEII phase-2 intercomparison. *Atmospheric Environment*, 115, 553-568, <https://doi.org/10.1016/j.atmosenv.2014.11.066>, 2015.

Levelt, P.F., Hilsenrath, E., Leppelmeier, G.W., Oord, G.H.J. van den, Bhartia, P.K., Tamminen, J., Haan, J.F., and de Veefkind, J.P.: Science objectives of the ozone monitoring instrument. *IEEE Trans. Geosci. Remote Sens.* 44, 1199-1208, <https://doi.org/10.1109/TGRS.2006.872336>, 2006.